Explorative Analysis and Data Mining in Big Neural Data

Jennifer Linge

2015

LUND
UNIVERSITY

Master's Thesis
Biomedical Engineering

Faculty of Engineering LTH
Department of Biomedical Engineering

Supervisors: Frida Sandberg and Ulrike Richter

Abstract

Most motor actions are carried out by many neurons acting together in different areas of the brain. Recently, techniques have been developed and increasingly used that allow simultaneous recordings of the activity from a large number of neurons over time ranges as long as several weeks. At Neuronano Research Center (NRC) at Lund University, neural activity in rodents has been recorded using chronically implanted 128-channel electrodes. The targets are within areas that play a prominent role in the planning, monitoring and execution of movements and, consequently, are strongly affected by motor diseases such as Parkinson's disease.

The experiments conducted at NRC naturally produces a large amount of neural data. This master thesis work aims to perform feature extraction from that data, i.e., find a way to mathematically describe the disease states of the rodents without *a priori* knowledge of the states. This is done by extracting features from the recordings, whose values later are used to analyse and cluster the data. The results show that a clear majority of the neurons exhibit a significant difference in feature values between the disease states. This means that it is possible to mathematically describe the different disease states. Moreover, the results show that different neurons behave differently: Some, e.g., exhibit increased activity going from one state to another, while others exhibit decreased activity. Adding to this, some does not exhibit any change while others exhibit a significant change.

That it is possible to mathematically describe the different disease states, with a timescale of hours, indicate that the same may be possible for states with smaller timescales. These states, with a smaller timescale, do not have to be connected to Parkinson's disease but could rather be normal, healthy states such as locomotion or reaching.

Contents

List of Figures

List of Tables

1

Introduction

Most motor actions, as well as sensory and cognitive functions, are carried out by many nerve cells, or *neurons*, acting together in different areas of the brain [1]. In recent years, techniques have been developed and increasingly used to record the activity from a large number of neurons, either individually or together as a population. The activity from a population of neurons can either be in the form of a summed activity or in a set of activity from related neurons recorded in parallel. It is not yet clear what knowledge can be gained from these recordings or if studying a population of several neurons, as opposed to studying one single neuron, can bring new insights to how the brain processes and executes information. There are, though, many reasons for wanting to study a population of neurons acting together rather than just one of these separately. In some cases, data recorded from one single neuron is not sufficient because the final action involves coordination of responses across multiple neurons. To study one neuron separately may even, in a worst case scenario, mislead or confuse in the search for the biological mechanism behind the neural activity. But, whether the data consists of activity from one single neuron or many acting together simultaneously, the need for ways to handle and interpret this massive amount of data, also called *big data* [2], is apparent.

To extract information from big data one can make use of an analytic process known as *data mining* (see Sec. 2.2). The ultimate goal of data mining is prediction or description [2]: During prediction, unknown variables or future values of variables can be predicted based on known values. During description, one finds patterns in the data that is presented in a form which is easily understood by humans [3].

This is one of the things that the group for Integrative Neurophysiology (Department of Experimental Medical Science and Neuronano Research Center, *NRC*) at Lund University, hopes to do. The group is pursuing rodent experiments, using chronically implanted electrodes to record neural activity within the *cortico-basal ganglia-thalamic loop* (see Sec. 2.1). The basal ganglia are known to play a prominent role in the planning, monitoring and execution of movements and in addition, they are strongly affected by motor diseases such as *Parkinson's disease* (see Sec. 2.1) [4]. For these reasons, the collection of deep brain structures has been chosen as a target for recordings in research projects addressing questions related to normal motor control of simple and complex movements. In this work simple movements include movements that involve most of the body and require gross motor control, for example straight locomotion and left or right turns, while complex movements such as reaching require a higher level of coordination and timing.

Research projects connected to the experiments at NRC, which this thesis is based on, also address questions related to motor dysfunction in Parkinson's disease. The majority of patients suffering from Parkinson's disease is treated with a drug called *levodopa*, but unfortunately a long-term usage of this drug results, for most of the patients, in severe motor complications [5]. These complications include abnormal involuntary movements collectively referred to as *levodopa-induced dyskinesia*. To attempt to identify the neurophysiological mechanisms underlying parkinsonian symptoms as well as levodopa-induced dyskinesia, the group at NRC has recorded activity in the related circuits over extended time periods during normal, parkinsonian, and dyskinetic states in awake freely behaving rats.

Common to all the projects related to the experiments conducted at NRC is the assumption that there is a dynamic change in the neural activity that can be related to changes between different behavioural or disease states. These dynamic changes could, e.g., be an increase of intensity, i.e., an increase in number of *action potentials* (see Sec. 2.1) fired. The timescale, or the dynamic changes, can vary from a subsecond up to several hours; while subsecond timescales can

include complex movements such as reaching, the different states of grooming can last for up to a few seconds, locomotion can take place during seconds up to a few minutes, and the disease states may occur in a timescale of up to one hour or even longer.

The overall goal of this master thesis is to explore methods for feature extraction from the neural activity recorded in the projects mentioned above, especially projects addressing questions related to the motor dysfunction in Parkinson's disease. Some of the features may be applicable for multiple timescales whereas others may be restricted to small *or* large timescales. Ideally, the feature identification will allow for the data to be clustered into different neural states, which in turn also allow a conclusion on the corresponding behavioural or disease states. The main focus will be on single- and multi-unit data (data recorded from one single neuron and several neurons, respectively) and the approach is, to begin with, purely data-driven. This means that it does not require *a priori* knowledge of the underlying behavioural or diseased states. To be clear, this is opposed to a classification-driven approach where the underlying states are known *a priori* and used in the training of a classifier.

2

Background

This chapter includes both medical and mathematical theory needed for this thesis work. The medical background includes Sec. 2.1 about the nervous system, with information about Parkinson's disease. The mathematical background includes Sec. 2.2 about data mining and Sec. 2.3 about spike trains and Poisson processes.

2.1 The Nervous System

The nervous system is a rapid control system that, together with the endocrine system, regulates and coordinates the cells of the human body [4]. It consists of a trillion of neurons that constitute the network of the brain, spinal cord, and periphery. These cells communicate with each other by means of chemical and electrical signals.

Neurons

There is a large diversity of neurons: They can vary in, e.g., size, shape and firing properties [4]. But even though they occur in a large variety there are still properties they all share. Among these are the overall anatomy and behaviour, both described below, and that they share features that allow for the cell-to-cell communication mentioned above.

A neuron consists of a cell body, or *soma*, containing the nucleus and ribosomes, and is surrounded by a membrane [6]. It has two types of extensions, the *dendrites* and the *axon*, through which it receives and sends information in the form of electrical signals. While a neuron can have many dendritic extensions, used to receive and process input information, its output is sent along a single extension, i.e., the axon.

The axon of a neuron is connected to the dendrites of one or several other neurons by junctions called *synapses*. When a sufficiently strong electrical signal (i.e., an action potential) reaches the synapses at the end of an axon, it causes the release of chemical messengers called *neurotransmitters*. After this release, the neurotransmitters reaches the dendrites of the *postsynaptic* neurons, where they are received by *receptors* and translated back to electrical signals that can be propagated further to the soma of each of these neurons [4]. The neurotransmitters can be both excitatory and inhibitory and hence they decide the final strength of the signal reaching the neuron's cell membrane. The anatomy of two connected neurons as well as a visualisation of a propagating action potential can be found in Fig. 2.1.

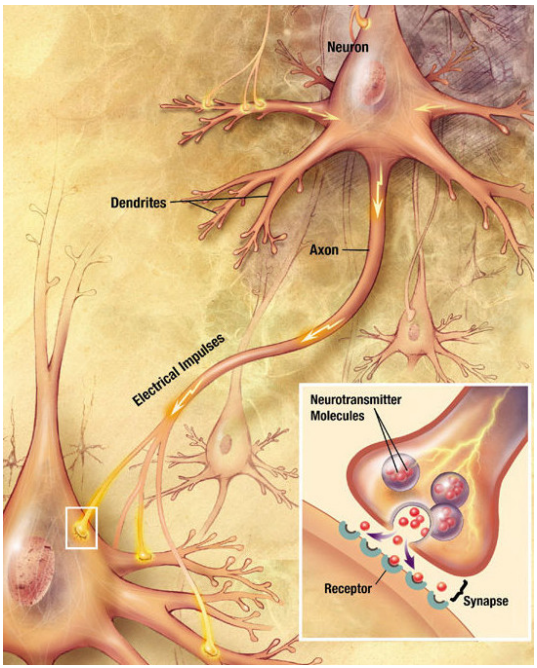

Figure 2.1: Visualisation of an action potential travelling between neurons [7].

Before the signal reaches the membrane of a neuron, a summation of incoming signals is made. The amplitude of the resulting signal is decided by (1) the total number of received signals, (2) how close these signals are to each other in time and (3) how far away from the soma they have been received. The input signals can be both excitatory, increase the membrane potential, and inhibitory, i.e., decrease the membrane potential. The level to which the membrane potential is raised increases with more excitatory signals as well as with an increased number of signals per time unit. An increase of membrane potential, from its resting state, is called *depolarisation*, the return (i.e., decrease of membrane potential) to the resting state after a depolarisation is called *repolarisation*, whereas a *hyperpolarisation* has occurred if the membrane potential is decreased *below* its resting state [8]. If the amplitude of a summed signal raises the membrane potential to a certain threshold it makes the receiving neuron fire an action potential. An approximate plot of an action potential showing the different states can be found in Fig. 2.2.

Action Potentials

Action potentials are the main part of the "booster system" that has evolved to conduct signals over great distances to amend the rather poor electrical properties of neurons. The potential over the cell membrane is measured as the difference between the interior of a neuron and the surrounding extracellular medium, and typically of the size -100 to $+40$ mV [9]. For the receiving neuron to fire an action potential, the incoming signal must raise the membrane potential of the neuron to its specific *threshold potential*, see Fig. 2.2. Action potentials is of great importance because they are able to travel rapidly over large distances without being attenuated, which is in contrast to sub-threshold potential fluctuations [8].

When an action potential is fired it is in the form of a very brief (~ 1 ms) change of membrane potential from negative to positive [9]. Action potentials are *all-or-none* events, meaning that either they occur fully or not at all. Here, fully means that all action potentials from a given cell have a stereotypical shape and duration, see Fig. 2.2 for a schematic example. The amplitude and duration of an action potential does not depend on the magnitude of the current that induced it, i.e.,

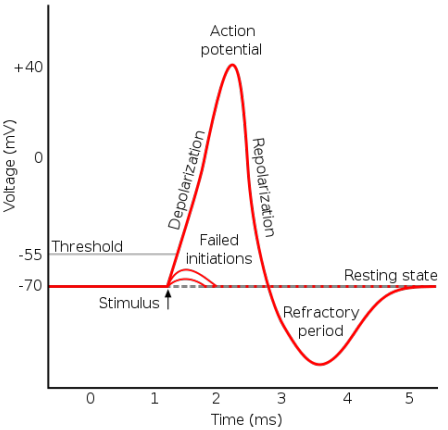

Figure 2.2: Approximate plot of an action potential showing the different states of polarisation [10].

larger currents does *not* give rise to larger action potentials. However, stimuli causing larger currents result in multiple action potentials being fired: An increased strength in stimulus causes an increased amount of fired action potentials. This means that the intensity of a stimulus can be measured through the amount of action potentials fired as a response to the stimulus, rather than by their amplitudes, shapes and durations. Different neurons fire action potentials with different *firing rates*; However, there is an upper limit for all neurons [8]. This upper limit is decided by the *refractory period*, see Fig. 2.2. The refractory period has a duration of a few milliseconds, during which it is impossible for another action potential to be fired.

Motor Control and The Basal Ganglia

The brain, as part of the nervous system, can be divided into the following subdivisions: the *medulla*, the *pons*, the *cerebellum*, the *midbrain*, the *diencephalon*, and the *cerebrum* [4]. Of these, the cerebellum and cerebrum and their descending pathways are the ones that are mainly involved when the brain processes and executes information concerning movement. The cerebrum consists of the right and left *cerebral hemispheres*, which have an outer layer called *cerebral cortex*, or *gray matter*, and an inside of *white matter*. The gray matter mainly

contains the cell bodies and synaptic connections while the white matter mainly contain the axons (see Fig. 2.3 for coronal slices of the cerebrum). The cerebrum furthermore comprises a number of deeper structures, such as the *subcortical nuclei* and the *thalamus*, which are interacting with the cerebral cortex.

The cerebral cortex plays a very critical role in controlling ongoing voluntary movements as well as planning them. It consists of different parts that together, as a whole, act to control muscle movements. Even though these parts are anatomically parted and functionally different they are heavily interconnected: One single movement may be controlled by neurons from different parts of the cerebral cortex and any one neuron may take place in several different movements.

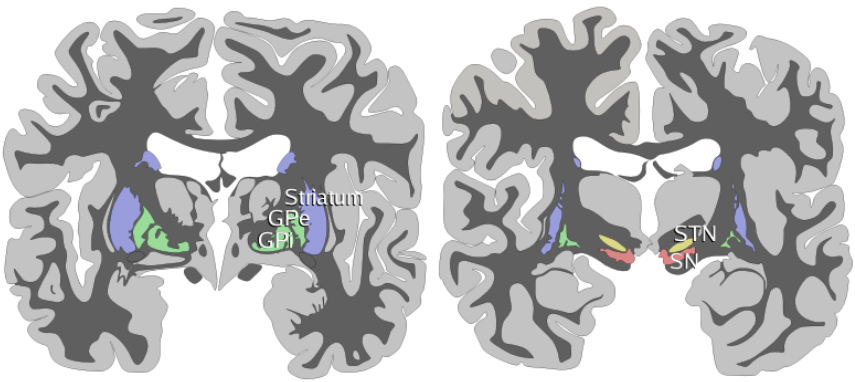

Figure 2.3: Location and anatomy of the basal ganglia in the human brain; (coloured) the basal ganglia, (dark gray) white matter, (light gray) gray matter, striatum, (Gpe and Gpi) globus pallidus, (STN) the subthalamic nucleus, (SN) substantia nigra. Note that the STN and SN lie farther back (posteriorly) in the brain than the striatum, GPe and GPi do [11].

The subcortical nuclei can be found in the very inner parts of the cerebrum. Among these, the *basal nuclei*, or so also called *basal ganglia*, are the most prominent structure [4]. The basal ganglia consist of the *striatum*, the *pallidum*, the *substantia nigra* and the *subthalamic nucleus*. These deeper structures, shown in Fig. 2.3, play a prominent role in the planning and monitoring of movements by establishing the pro-

grams that determine all parts of a movement to complete an action. The basal ganglia form a link in the circuits that transmit the activity in the motor system, some of which facilitate movements and others suppress movements, thereby keeping the balance between voluntary and involuntary movements. It is during certain disease states, such as Parkinson disease, that the importance of the proper functionality of the basal ganglia becomes most evident.

Parkinson's Disease

Parkinson's disease is the second most common degenerative disease (Alzheimer's disease being the most common one) and is characterised by a reduced amount of movement, so called *akinesia*, slowness of movements, termed *bradykinesia*, rigidity in the muscles (extremities and neck), minimal facial expressions and a tremor at rest [4, 9]. The disease is also associated with dementia and the onset is gradual, usually between the ages of 50 and 70 [9]. After this it progresses slowly, leading to death 10 to 20 years later.

In a Parkinson patient the balance between the circuits facilitating and suppressing movements is impaired, and activation of the motor cortex is reduced [4, 9]. This is due to an initial defect in the neurons of the substantia nigra in the midbrain, more precisely consisting of a loss of dopaminergic neurons (neurons related to the neurotransmitter dopamine [12]). The degeneration of these neurons causes a decreased amount of dopamine to be delivered to the basal ganglia, which in turn decreases the activation of the motor cortex, i.e., the region of the cerebral cortex that controls muscle movement. The cause of the degeneration of these cells and the subsequent development of Parkinson's disease is still unknown [4]. The majority of Parkinson cases are sporadic, but some cases indicate that the disease may be inherited. Some research has, in addition, shown that exposure to environmental toxins may play a roll in the causing of the disease.

Today, Parkinson's is treated with drugs that are all designed to restore dopamine activity in the basal ganglia. The most widely prescribed drug is the dopamine precursor levodopa (*L-dopa*). Unfortunately new problems arise with long-term use of levodopa; it results in severe motor complications for most patients [5]. These motor complications

consist of abnormal involuntary movements with hyperkinetic ("fast-paced or frenetic activity" [13]) or dystonic ("any of various conditions characterised by abnormalities of movement and muscle tone" [14]) features and are collectively referred to as levodopa-induced dyskinesia.

2.2 Data Mining

Recordings of neurons often result in a large amount of data to analyse. To tackle this size problem one may make use of data mining, which has been developed as a natural result of the ever increasing amount of data [3]. It is extensively used to identify phenomena concealed in data, not just in neural data, faster and better than human experts. The aim of data mining is to extract previously unknown and potentially useful information from data, i.e., to *predict* or *describe*. Data mining generally consists of three phases [2]; (1) exploration, (2) model building and validation and (3) deployment. A general description of all phases follow below.

Exploration The exploration phase usually involves preprocessing of the data [2]. The preprocessing could be to apply transformations, select subsets of the recordings, or to perform preliminary feature extraction to keep the number of variables to a manageable size. After the preprocessing the most relevant variables are identified, followed by the determination of complexity and/or general nature of the models that are to be taken into consideration in the next phase.

Model Building and Validation In this stage, the model with the best predictive performance is chosen among others proposed in the previous phase [2]. This choice is generally made after application of all models to the same data. The predictive performance is measured in the model's ability to explain the variability in question and produce stable results across samples. When the superior model has been chosen it is applied to other data to validate its performance.

Deployment During the deployment phase, the model chosen in the previous phase is applied to data sets of interest in order to

generate predictions or estimates of the expected outcome [2]. If the data mining has been successful, this is where it reaches its ultimate goal, i.e., prediction or description.

Prediction methods use some known values to predict unknown or future values of variables. There are different kinds of prediction methods, e.g., *classification*, *regression* and *deviation detection* [3]. Description methods aim to find patterns that can describe the data in a human-understandable way. Examples of description methods include, e.g., *clustering*, *association rule discovery* and *sequential pattern discovery*.

2.3 Spike Trains and Poisson Processes

As mentioned earlier in this chapter, action potentials convey information through the frequency of their firing, or their timing [8]. Because action potentials are very stereotypical they can mathematically be treated as identical events. Adding the fact that they have a very short duration, they can be approximated as delta pulses, or *spikes*. As a result of this, a sequence of action potentials fired can be described as a sequence of the time instances for each spike occurrence, a so-called *spike train*.

A spike train can be visualised as a series of ones and zeros, where a one would mean a spike occurred and a zero that no activity was recorded. Adding a time resolution to the sequence , i.e., a fixed time period that passes between every one or zero, reveals the firing rate of the spike train. With a high time resolution, several ones in a row indicate high firing rate, whereas if there are many zeros between each one, the firing rate is low. When high-frequency firing-rate fluctuations occur one may wonder whether the pattern of these carry any significant information. If so, the question of how precisely the spike times must be measured arises, and with this *temporal coding* [8]:

To understand the difference between temporal- and rate coding, consider the two spike trains stated below.

0	0	0	1	1	1	1	0	0	1	0	1	1	1	0	0
0	1	0	1	0	1	0	1	0	1	0	1	0	0	1	1

As both of these spike trains contain eight spikes during the time observed, calculating the mean firing rate would give the same result for the first as for the second. However, when looking at the sequence of ones and zeros it is obvious that they are different. As opposed to the measure of mean rate, a temporal code would tell them apart. The question whether firing patterns reveal information on small (millisecond) time scales has given rise to different measures that interpret the information spike trains carry. Some of these are purely based on the firing rate, whereas others aim to make an interpretation that is less dependent of the same.

The Statistics of a Spike Train

One way to characterise a spike train is by the use of statistics [8]. A good place to start is to consider the probability of a spike occurring during a time interval, $t + \triangle t$. The probability that a spike occurs during this interval is proportional to the size of the interval when $\triangle t$ is small. In fact, this relation holds for any continuous stochastic variable. That is, for any continuous stochastic variable X, the probability $P[x]$ that X takes the value x in the interval $x' + \triangle x$, for small $\triangle x$, is $p[x]\triangle x$, where $p[x]$ is the probability density. With this terminology we can express the probability that a certain spike train occurs as

$$P[t_1, t_2, ..., t_n] = p[t_1, t_2, ..., t_n](\triangle t)^n \tag{2.1}$$

where n is the number of spikes during one time period T and t_i the time instances for each spike in the interval $[0, T]$. The problem, though, with trying to estimate the probability for a certain spike sequence to occur is that the number of possible spike sequences usually is very large. So large, that even a rough estimation can be considered impossible. To still be able to characterise the sequence in some way one can make use of *point processes*.

Point Processes and the Poisson Process

A point process can in short be described as a process that simply consists of points in time. Each point can be seen as a certain event in time, such as the occurrence of an action potential [15]. Generally, the probability of any event to occur at a certain point in time could depend on the entire history of all events that has occurred before that event. If this dependence only extends as far as to the preceding event, the process is called a *renewal process*. It is among these processes that we find a certain kind of process that makes an "extremely useful approximation of stochastic neuronal firing" [8]: The *Poisson process*.

A formal definition of a Poisson process by [15] reads

Definition 1. *A Poisson process with intensity* $\lambda > 0$ *is a stochastic process* $\{N(t),\ t \geq 0\}$*, such that*

(i) $N(t)$ *is integer valued, growing and* $N(0) = 0$*,*

(ii) $N(t)$ *has independent and stationary increases,*

(iii) $N(t) \in Po(\lambda t)$*.*

The one-dimensional probability density function for the Poisson process, which determines the probability for x spikes to occur within the time interval $[0, t]$, is defined by

$$p_{N(t)}[x] = e^{-\lambda t}\frac{(\lambda t)^x}{x!}, \quad x = 0, 1, \ldots . \tag{2.2}$$

There are two types of Poisson processes: homogeneous and inhomogeneous. Homogeneous Poisson processes have constant intensity λ, whereas in inhomogeneous ones the intensity changes over time: $\lambda = \lambda(t)$ [8]. The focus will be on the homogeneous Poisson process and on taking steps that show the connection between its distribution and the modelling of spike trains as stochastic processes.

Spike Trains and the Homogeneous Poisson Process

The intensity of a spike train is the rate, r, at which the neuron fires action potentials [8]. A constant firing rate means that the process

generates every sequence of n spikes, within a fixed time interval, with equal probability. It is possible to express the probability of a certain spike train $P[t_1, t_2, ..., t_n]$ using the probability of an arbitrary sequence of exactly n spikes occurring within the fixed time interval T: $P_T[n]$. The use of $P_T[n]$ to formulate an expression for a certain spike train calls for a conditional probability with a condition on the number of spikes within the time interval $[0, T]$. Recognising this, one can make use of the following theorem from [15].

Theorem 1. *Let $T > 0$. The conditional distribution for the events in $(0, T]$ given $N(T) = n$ is the same as for n points that are independently and uniformly distributed over $(0, T]$.*

With use of this theorem and remembering that n spikes can be sorted in $n!$ number of ways, $p[t_1, t_2, ..., t_n]$ in equation (2.1) can be expressed as $n!\, P_T[n] \frac{1}{T^n}$. Using this, equation (2.1) becomes

$$P[t_1, t_2, ..., t_n] = n!\, P_T[n] \left(\frac{\triangle t}{T} \right)^n . \tag{2.3}$$

Now, to finalise the expression for the probability $P[t_1, t_2, ..., t_n]$ of a certain spike train to occur, an expression for $P_T[n]$ is needed. To find this expression, it is convenient to divide the time interval T into M bins of the same size $\triangle t = T/M$. At the end of the process of finding an expression for $P_T[n]$, the limit $\triangle t \to 0$ will be applied, and for this reason one can assume that $\triangle t$ is so small that two spikes will never occur within a single bin. The expression for $P_T[n]$ can now be constructed by multiplying three factors:

1. the probability of $n \leq M$ spikes to occur within a subset of M bins

2. the probability of spikes to *not* occur in the $M - n$ remaining bins

3. the number of possible ways to put n spikes into M bins

The first factor becomes clear when considering that the probability of a spike to occur in one specific bin is $r\triangle t$ and, because of the independence, the probability of n spikes to occur in n specific bins is $(r\triangle t)^n$. The same reasoning can be applied to the second factor with the probability of a spike to not occur in a bin being $(1 - \triangle t)$, i.e. the second factor can be expressed as $(1 - r\triangle t)^{M-n}$. Finally, the third factor is given by the binomial coefficient $\binom{M}{n}$. These three factors together create the expression for $P_T[n]$:

$$P_T[n] = \lim_{\triangle t \to 0} \frac{M!}{(M-n)!\, n!} (r\triangle t)^n (1 - \triangle t)^{M-n}. \tag{2.4}$$

As $\triangle t \to 0$, M grows without bound (recall $M\triangle t = T$, and T is fixed). The fact that n also is fixed lets us approximate $M - n \approx M = T/\triangle t$, and by introducing $\epsilon = -r\triangle t$ the limit of the third factor becomes obvious:

$$\lim_{\triangle t \to 0} (1 - r\triangle t)^{M-n} = \lim_{\triangle t \to 0} \left((1+\epsilon)^{1/\epsilon} \right)^{-rT} = e^{-rT}. \tag{2.5}$$

For large M, $M\,!/(M-n)! \approx M^n = (T/\triangle t)^n$, and finally the expression for $P_T[n]$ can be stated as

$$P_T[n] = e^{-rT} \frac{(rT)^n}{n\,!} \tag{2.6}$$

which can be recognised as the Poisson distribution from equation (2.2) with $\lambda = r$, $t = T$ and $x = n$.

The use of the Poisson process to describe the probability of an arbitrary sequence of exactly n spikes in the interval T ($P_T[n]$) seems reasonable when noting that for increasing values of n, the process reaches its maximum at larger values of T [8]. This means, in reality, that if a large number of spikes is desired, a larger T should be chosen to maximise the probability for this to happen. This is illustrated by Fig. 2.4, where the probability of a number of spikes to occur is shown as a function of rT. In fact, the Poisson process is the most frequently

used type of stochastic point process when dealing with neuronal modeling [16]. One important reason is that it is simple enough to allow generation of computer simulated spike trains, while still not being too far from real life spike trains that have been recorded from physiological neurons.

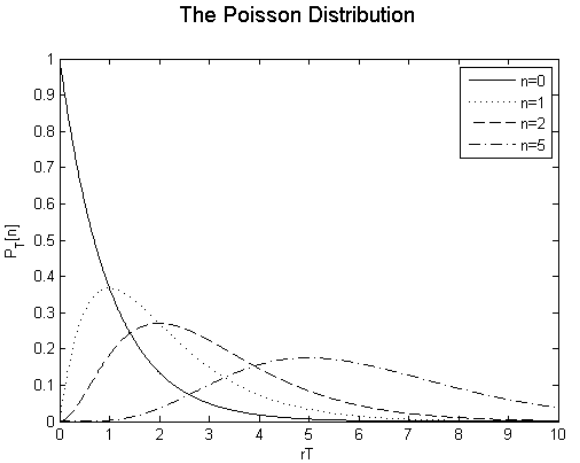

Figure 2.4: The Poisson distribution for different number of spikes (n) as a function of the rate (r) multiplied by the time period (T).

3

The Experiments at NRC

At NRC, the experiments are conducted on rats. The reason for this is that rodents share many similarities with humans in organ structure and function. Because of this more than 90% of today's medical research is done on rodents [17]. The advantages with using rodents also include their small size, high reproduction rate, low cost and easy handling.

During the experiments, neural data was recorded from both healthy and *hemi-parkinsonian* rats by use of implantable electrodes. The hemi-parkinsonian rats recieved, three weeks prior to the electrode implantation, injections into the right hemisphere according to the unilateral Parkinson model (see [17]). Thus, the left hemisphere remains healthy and could be used as a reference, while the right hemisphere becomes parkinsonistic. Two weeks after lesioning, moderate motor impairments were apparent.

3.1 Electrodes

The design of the novel electrodes used at NRC faces many challenges [17]. It has to be possible to mount the electrode on the small surface of the rat's skull and the rat must be able to carry it during the long periods of time that the experiments are conducted under, i.e., it has to be compact and light. It needs to be implantable in a single surgical procedure, i.e. it has to be built in one single piece with a high precision for each target structure, and it has to record a multiple number of channels in the target structures. In addition, the implantation of electrodes into different brain structures often involves the concern

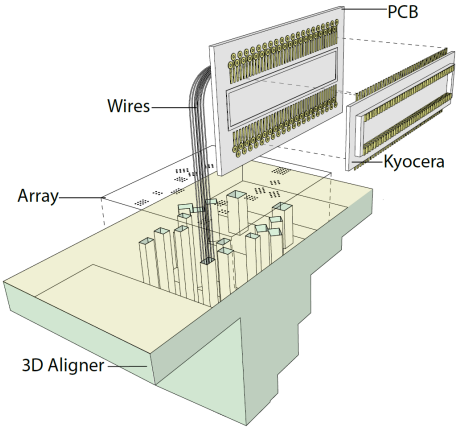

Figure 3.1: Schematic overview of design assembly in its near-to-end stage. The three-dimensional (3D) aligner and two-dimensional (2D) array ensure that the wires are positioned correctly [17].

of different vertical positions of the targets, which further complicates the production process. Fig. 3.1 shows a schematic overview of the design solving the last stated problems [17]: A three-dimensional aligner and two-dimensional array assure that each channel is recorded from the correct vertical and *anterolateral* (situated in front and to one side [18]) positions. The anterolateral and vertical coordinates for the correct positions were retrieved from the literature after decision about the desired targets (see Fig. 3.2 for the placement of the electrode targets). The design assembly in Fig. 3.1 is close to its end stage.

Currently, the design of the electrodes used for recordings at NRC allows for 128 recording channels and thus large amounts of data to be recorded from one single animal during a time span reaching from several weeks up to two months [17]. They include extracellular single- and multi unit data and local field potentials (the summed activity of many thousands of neurons close to the tip of the electrode). Further, it allows the animal to be awake and behave freely, rather than being anaesthetised or restrained in its mobility. In fact, the choice of the targets for recordings at NRC has been such that neural activity in all structures of the basal ganglia circuit of an awake, freely behaving

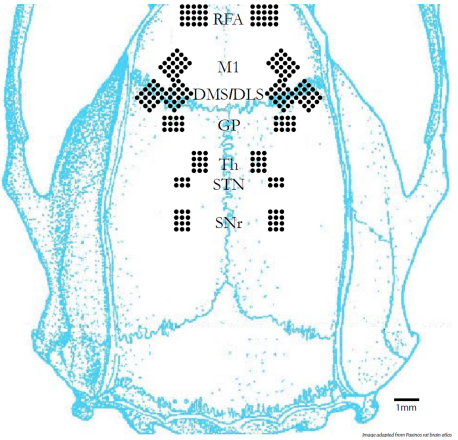

Figure 3.2: Dorsal view of the rat skull showing the placement of the electrode targets in the cortico-basal ganglia-thalamic circuit. The electrode spacing is 250 μm. Included sites are the rostral forelimb area (RFA), primary motor cortex (M1), dorsolateral striatum (DLS), dorsomedial striatum (DMS), globus pallidus (GP), thalamus (Thal), subthalamic nucleus (STN) and substantia nigra pars reticulata (SNr). [17].

rat has been recorded in parallel for the first time [17]. Details on the surgical procedures for electrode implantation can be found in, e.g., [5, 17].

3.2 Experimental Setup

The experiments are conducted in one of two ways: (1) During an *open field recording* a healthy animal is placed in an enclosed square area, 75x75 cm, and its behaviour recorded for an extended amount of time, up to several hours and (2) During a *dyskinetic recording* the animal is placed in a transparent cylinder with a diameter of 250 mm and recorded for 30 min to establish baseline conditions. After this the animal is injected with levodopa and the recording continues until the dyskinesia diminish spontaneously. During the dyskinetic recordings the dyskinesia usually develops 10 to 20 min post-levodopa, reaches its peak around 60 min post-levodopa and diminishes about 2

h post-levodopa. During all experiments, the behaviour is documented through video in parallel with electrophysiological recordings.

3.3 Data Acquisition

For recordings, the implant was connected to head-stages and cables of the 128-multi-channel recording system [5, 17]. The cables were attached to a multi-channel commutator, which allow the animal to move freely during the experiment. The sampling frequency of the recording system was 32 kHz. The signals were then directly preprocessed in two different ways to obtain unit activity (action potentials) and local field potentials in parallel. The unit activity was obtained through high-pass filtering at 600-9000 Hz and applying threshold detection. For every threshold crossing, its time point as well as 32 samples (i.e., 1 ms) of the signal, representing the waveform of the putative action potential, were saved for subsequent offline-sorting, see Sec. 3.3. In this thesis work, only the unit activity was employed for further analysis. The animal's movement was also recorded with a monochrome video camera. A Master-8 pulse generator was used to synchronise the sampling of the neural and video recordings.

Spike Sorting

In every channel, the waveforms of the putative action potentials were sorted into single/multi units (signals recorded from one and several neurons respectively) or noise through automatic clustering with slightly modified algorithms from the Chronux toolbox [19]. All automatically generated clusters were manually reviewed at the NRC to determine if clusters, waveforms and interspike-interval distributions were physiologically plausible. Clusters were only modified by merging and splitting them according to the cluster hierarchy imposed by the algorithm.

3.4 Datasets

The data used in this thesis work consists of neural data from 4 different recordings: 2 sets from dyskinetic recordings, with hemiparkinsonian rats (Dyskinesia Recording 4 and 7) and 2 sets from

open field recordings, with healthy animals (Open Field Recording 8 and 36). Within each data set there are recordings from a collection of neurons, individually recorded with time stamps for each action potential fired, as well as time stamps for events such as, e.g., the injection of levodopa or start and stop of locomotion.

The main focus of this thesis is on the recordings from the hemi-parkinsonian rats, and therefore the data obtained from these rats is presented in greater detail in Table 3.1. The table shows the number of neurons, and their sites, that were recorded for Dyskinesia Recording 4 and 7.

# **Neurons**	Left/Right	Dyskinesia Rec. 4	Dyskinesia Rec. 7
All	L & R	15	106
	L	12	71
	R	3	35
RFA	L	2	10
	R	0	3
M1	L	2	11
	R	0	11
DLS	L	0	3
	R	3	6
DMS	L	2	8
	R	0	9
GP	L	5	29
	R	0	2
Thal	L	0	3
	R	0	2
STN	L	0	1
	R	0	1
SNr	L	1	3
	R	0	0
Unknown	L	0	3
	R	0	1

Table 3.1: Table presenting the site and number of neurons recorded for Dyskinesia Recording 4 and 7. Sites included are rostral forelimb area (RFA), primary motor cortex (M1), dorsolateral striatum (DLS), dorsomedial striatum (DMS), globus pallidus (GP), thalamus (Thal), subthalamic nucleus (STN) and substantia nigra (SNr).

4

Methods

This chapter describes the methods that were used in this thesis work. It starts, with Sec. 4.1, by describing the notations and terminology that will be used from now on and continues with descriptions of how the data is handled in Sec. 4.2. After these introductory sections the features, in Sec. 4.3, the process of principal component analysis, Sec. 4.4, clustering, Sec. 4.5 and classification, Sec. 4.6, will be described.

4.1 Notations and Terminology

During each experiment, data is gathered both through video and neural recordings. Each such experiment will be referred to as a *trial*. The collection of timestamps gathered over the whole duration of a trial for one neuron will be referred to as a *recording*. This means that for each trial, there will be several recordings, one for each neuron, as well as video material and event information. The event information is, as described in Sec. 3.2, timestamps for the injection of levodopa, and for the open field recordings start and stop of locomotion.

Each recording will be defined by timestamps for the action potentials recorded from a specific neuron. These will be denoted by t, meaning a recording can be expressed as $[t_1\ t_2\ t_3\ ...\ t_N]$, where N is the total number of spikes that neuron fired. The number of spikes within a time period will simply be denoted by n. Note that each neuron may fire a different total number of spikes, N.

From the timestamps vector, t, a vector containing the *interspike intervals* (ISIs), can be computed. A certain ISI is defined as the time difference between two consecutive action potentials and is denoted with τ. Hence, a more formal definition of the ith ISI is $\tau_i = t_{i+1} - t_i$ and the ISIs over a whole recording is $[\tau_1\ \tau_2\ \tau_3\ ...\ \tau_{N-1}] = [t_2 - t_1\ \ t_3 - t_2\ \ t_4 - t_3\ \ ...\ \ t_N - t_{N-1}]$.

For calculation of the measurements, a recording will be divided into *segments*. Each segment consists of the spikes within a certain time period, which will be denoted by T. All segments will be further divided (or *binned*) into smaller segments of time, which will be referred to as *bins* (see Sec. 4.2). To obtain higher time resolution an overlap over the segments is implemented and for each segment, a value for every feature in Sec. 4.3 below is calculated.

4.2 Segmentation

The datasets used in this thesis work is in the form of *single trials*. Many methods and measures are formulated to be applied to data created using *repeated trials*, as opposed to one single trial. When using repeated trials one knows what is happening and when. It could, e.g., be the recording of a rat that has been taught to act in a certain way when a light goes on. The recording could start just before the light goes on and be stopped after enough time has passed to record the reaction of the animal. Making several trials like this enables one to establish a general characteristic of the response over time. To do this it is common to align the trials and calculate the mean over the trials for each time point.

In a single trial recording one can not average the response to eliminate artifacts or noise components. One advantage of averaging over trials is that it can result in a more robust estimation of the response. The reason why this kind of averaging is not possible to perform for single trial recordings is that one may not have several occasions when the same behaviour or action is recorded. Even if that exists, the time points for these occasions can be unknown and the actions could be results of different stimuli or circumstances.

Having mentioned this, there are still ways to apply measures based on this kind of averaging to single trial recordings. When doing so it is important to keep in mind that the analysis is not completely analogous to the analysis that can be performed for repeated trials. Two methods, described below are used here to resolve the problems faced when dealing with single trials.

Time Segmentation

Each recording is divided into segments with a fixed time duration and a certain overlap to allow for higher time resolution. Each segment is further divided into non-overlapping bins with a shorter time duration to allow for the averaging performed for repeated trials, i.e., after applying a measure separately to the data in each bin of a segment, the average measure for the segment can be calculated. The process of time segmentation, using zero overlap for the segments, is illustrated by Fig. 4.1.

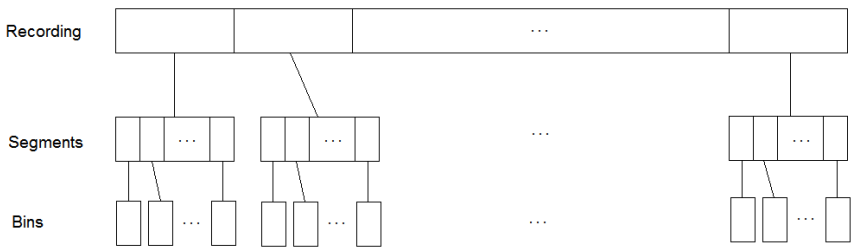

Figure 4.1: Illustration of the time segmentation of the data with zero overlap between segments.

This procedure was used for Dyskinesia Recording 4 and 7 after the removal of data close to the injection of levodopa. The segmentation was made using a sliding window of length 120 s, with 87% overlap. The bin size were 5 s and no overlap was used when binning within the segments.

Trigger Segmentation

A certain kind of event is chosen as a trigger, e.g., start or stop of locomotion. Around each such event a time window with fixed time intervals before and after the event is applied. Doing this aligns the time windows, or *event recordings*, along the chosen event, see Fig. 4.2, and they can be used in the same manner as repeated trials. The event recordings is further segmented according to time segmentation. The mean values of the applied measures are calculated horizontally over the aligned bins from each and every segment in Fig. 4.2. The procedure of trigger segmentation was used for Open Field recording 8 and 36.

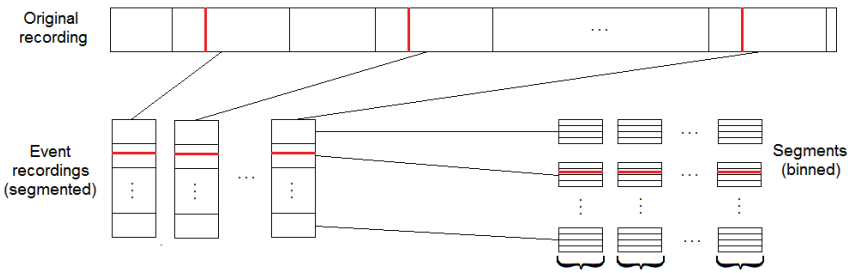

Figure 4.2: Illustration of the trigger segmentation of the data, showing the event times in red.

Exclusion Criteria

The largest disturbance in the recording process is the injection of levodopa. Around the injection, the animals experience stress. Because of this, the signals recorded close to the injection are not representative for the behaviours or states that one wishes to identify. Therefore, to simplify the calculations, 5 min before the injection are excluded from the data as well as 5 or 30 min after the injection. The reason for the choice of the longer time interval, 30 min, is that after that amount of time, the dyskinesia should be well developed. If one wishes to identify this state or differentiate it from the state before the injection it should

be easier if the state is fully developed as opposed to gradually growing. To perform calculation with data including the gradually growing dyskinesia, i.e. only 5 min of the data post injection removed, is unnecessary if no satisfactory results are obtained from the calculations performed on the data with only fully developed dyskinesia included.

Throughout the rest of this thesis work, the state before levodopa injection will be referred to as *baseline* or *pre-levodopa* state, while the state after levodopa injection will be referred to as *post-levodopa* state.

4.3 Feature Extraction

To tell disease states or behaviours apart, different measures are implemented over time. The states to be recognised include, primarily, the baseline from the post levodopa state and, secondarily, motor behaviour such as, e.g., start and stop of locomotion. This chapter presents all measures that have been applied to the data in the current work. The application of measures is the first step in the process of feature extraction and classification of behavioural or disease states.

Rate

As mentioned in Ch. 1, the variability of the firing rate of a neuron over time may convey information that can be used to reveal the underlying behavioural or disease state of the animal during the recording.

The firing rate, denoted r, is simply calculated by dividing the number of spikes, n, that has occurred during a certain time period T by the length of the time period.

$$r = \frac{n}{T}$$

The firing rate is low when there are few spikes per time unit and high when there are many, see 4.3. Note that during the time intervals where the firing rate is constant, e.g. $[0, 20]$ and $(40, 60]$ s, the lower plot does not show constant firing rate. This is a consequence of the timing of the segment edges relative to the spikes.

The rate was calculated for each bin and the features extracted from

each time segment the average, $< r >$, and variance, σ_r^2, over the bins within that segment.

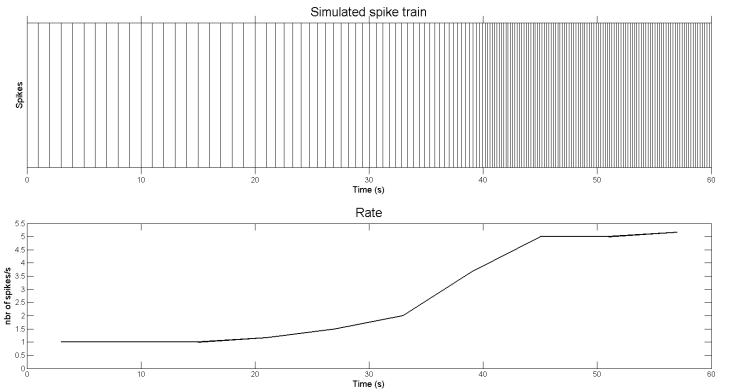

Figure 4.3: Visualisation of the firing rate (below) as a measure of a simulated recording (above). The recording is simulated with constant, low frequency $t = [0, 20]$, increasing frequency $t = (20, 40]$ and constant, high frequency $t = (40, 60]$.

Global Measures of Variability

Fano Factor The *Fano factor* (FF) is one of the most commonly used measures for estimating the variability of spike trains [20]. It is defined as the ratio of sample variance to sample mean of spike counts, and takes the value 1 for a homogeneous Poisson process, i.e., a Poisson process with constant intensity [8].

$$FF = \frac{\sigma_n^2}{\langle n \rangle}$$

where σ_n^2 denotes the variance and $\langle n \rangle$ the mean of the spike count.

The Fano factor is a measure of how alike a certain distribution is the homogeneous Poisson process. The length of the time window, T, has been documented to affect the estimator strongly. Unfortunately, it is not yet clear how to choose a suitable time window [20].

Coefficient of Variation The *coefficient of variation* (CV) is another commonly used measure for estimating the variability of spike trains [20]. When measuring the variability of a spike train it is often assumed that the spike train satisfies the definition of a renewal process (see Sec. 2.3), which is the case for CV.

The CV is based on the ISIs and calculated by the ratio of the square root of the variance of the length of these to their mean [8]:

$$CV = \frac{\sigma_\tau}{\langle \tau \rangle},$$

where σ_τ^2 is the variance of the ISIs and $\langle \tau \rangle$ their mean. Like the FF, the CV takes the value 1 for a homogeneous Poisson process, and hence it is also a measure of how alike the distribution of a spike train is to the homogeneous Poisson process.

In Fig. 4.4, three recordings has been simulated. The first one (left) was simulated with an underlying homogeneous Poisson process, the second (center) drawn from the standard normal distribution $N(0, 1)$, and third (right) created by using two different ISIs, which is visible in the histogram of the ISIs. Note that, in the third histogram, there are 40 ISIs that have the length of 1 s but they are so few that they are barely visible when compared to the large number (2000) of ISIs with length 0.1 s. As expected, the value of the Fano factor and coefficient of variation oscillates around 1 for the homogeneous Poisson process. The second and third simulations are examples of distributions having low respectively high values of the FF and CV.
As can be seen in the plots showing the FF and CV for the simulated homogeneous Poisson process, i.e. column 1 of Fig. 4.4, the value of the FF varies more than that of the CV. The values for the homogeneous Poisson process should in theory both be 1 since this is how the measures are constructed but this is not the case for all time segments. The reason for this is either the timing of the bins within a segment or that there are sudden changes in firing rate. Another recording, Fig. 4.5, was simulated to explain this further.

In Fig. 4.5, a recording with low constant firing rate in the interval $[0, 20]$, slowly linearly increasing firing rate in the interval $(20, 40]$

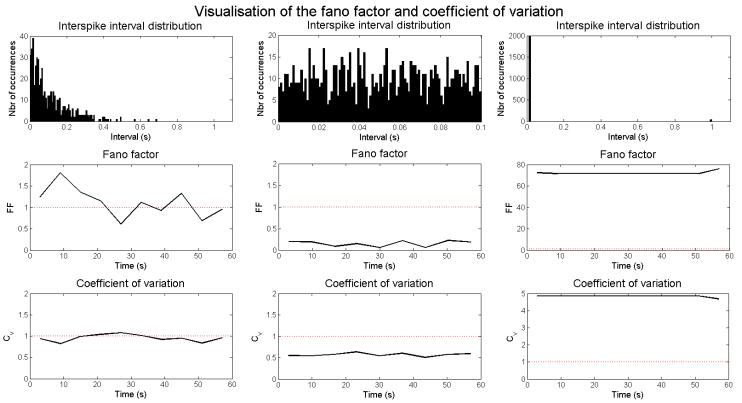

Figure 4.4: Visualisation of the Fano factor (middle) and the coefficient of variation (lower) as measures of simulated recordings with different interspike interval distributions (upper). The first simulated recording has an underlying homogeneous Poisson process, for the second the standard normal distribution was used and the third has two different rates, with ISIs of lengths 0.1 and 1 seconds.

and constant, high firing rate in the interval $(40, 60]$ has been simulated. One can clearly see that there are two peaks for both the FF and CV and that these are located close to where the firing rate is changed. Another thing that is worth mentioning is that the FF is 0 around 30 s even though the firing rate is changing. The reason for this is the timing of the bins within the segments in combination with the fact that the change of firing rate is small. Even though the firing rate is changing it so happens that there are the same number of spikes within every bin in these segments. When comparing this interval to the same interval for the CV one notices that the CV is not equal to 0 here. This is because even though there might be the same number of spikes within each bin the lengths of the ISIs are still different. This allows the CV to be a more accurate measure in this specific case.

As now has been made clear, the FF and CV are sensitive to sudden changes in firing rate. This may be somewhat troublesome since they are not meant to measure variability in firing rate. That the FF and CV changes as the firing rate varies is, unfortunately, a consequence of

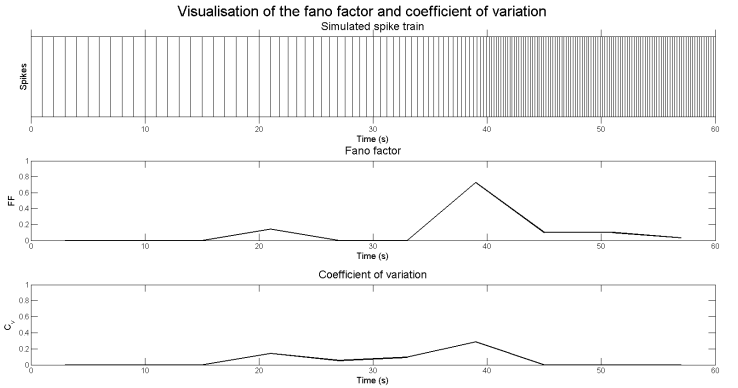

Figure 4.5: Visualisation of the global measures Fano factor (middle) and coefficient of variation (below) as measures of a simulated signal (above). The recording is simulated with constant, low frequency $t = [0, 20]$, increasing frequency $t = (20, 40]$ and constant, high frequency $t = (40, 60]$.

the formulation of the measures. What they are meant to measure is, as mentioned above, how alike a process is the homogeneous Poisson process: If the distribution is close to a homogeneous Poisson distribution, the FF and CV should be close to 1. That the FF and CV overestimate the variability when there are sudden changes in firing rate motivates the introduction of more local measures of variability. If a measure of variability operate on just a few spikes or ISIs they would not overestimate sudden changes in firing rate and the variability of slow changes in firing rate would be more accurately measured.

Local Measures of Variability

One problem with the FF and the CV, as stated above, is that they overestimate the variability when there are pronounced firing rate changes [21]. To avoid this problem, temporally local measures of spike time irregularity have been formulated. Four of these measures, that are more robust to firing rate changes, are described below. All four measures are based on consecutive ISIs, τ_i and τ_{i+1}. For each measure a metric m_i is introduced as a function of the consecutive ISIs. In general, a metric must be invariant to changing τ_i into τ_{i+1}, positive, and equal to zero only if $\tau_i = \tau_{i+1}$. Note that all metrics, and so also

the measures based on these, are functions of the ratio of consecutive ISIs. In practice, this means that they are scaled with the instantaneous firing rate and, because of this, relatively rate-independent.

The Local Coefficient of Variation The *local coefficient of variation* (CV_2) is the local version of the global measure CV, with the subscript indicating that it depends on only two ISI values. The metric of CV_2 is defined as [21]

$$m_i^{CV_2} = 2\frac{|\tau_i - \tau_{i+1}|}{\tau_i + \tau_{i+1}},$$

and the CV_2 by its average

$$CV_2 = \frac{1}{M}\sum_{i=1}^{M} m_i^{CV_2}.$$

The choice of M decides the number of segments for the whole duration of the recording.

The local coefficient of variation was calculated for each bin and the features extracted from each time segment the average, $< CV_2 >$, and variance, $\sigma^2_{CV_2}$, over the bins within that segment.

The Local Variation The *local variation* (LV) is a quadratic version of CV_2 based on the metric [21]

$$m_i^{LV} = 3\frac{(\tau_i - \tau_{i+1})^2}{(\tau_i + \tau_{i+1})^2},$$

and defined by the average

$$LV = \frac{1}{M}\sum_{i=1}^{M} m_i^{LV}.$$

The local variation was calculated for each bin and the features extracted from each time segment the average, $< LV >$, and variance, σ^2_{LV}, over the bins within that segment.

The Irregularity Measure The *irregularity measure* (IR) is a measure of irregularity of spike train data based on the metric [21]

$$m_i^{IR} = |\log(\tau_i/\tau_{i+1})|,$$

and defined by the scaled average

$$IR = \frac{1}{\log(4)} \frac{1}{M} \sum_{i=1}^{M} m_i^{IR}.$$

The choice of scaling factor as $\log(4)$ ensures that $CV_2 = LV = IR = 1$ for a Poisson process to fall in the same range as the global measure CV. The choice of scaling factor for the measure SI below will be due to this reason as well.

The local irregularity measure was calculated for each bin and the features extracted from each time segment the average, $< IR >$, and variance, σ_{IR}^2, over the bins within that segment.

The Spiking Irregularity Measure The *spiking irregularity measure* (SI) provides an estimate of the shape parameter of a spike train in a gamma-distributed assumption of spiking activity. The metric for SI is defined as [21]

$$m_i^{SI} = -\frac{1}{2} \log\left(\frac{4\tau_i\tau_{i+1}}{(\tau_i + \tau_{i+1})^2}\right).$$

To average the measure of M individual values, the following expression is used,

$$SI = \frac{1}{1 - \log(2)} \frac{1}{M} \sum_{i=1}^{M} m_i^{SI}.$$

The local spiking irregularity measure was calculated for each bin and the features extracted from each time segment the average, $< SI >$, and variance, σ_{SI}^2, over the bins within that segment.

A visualisation of the local measures of variability can be found in Fig. 4.6. The simulated signal is the same as the ones used in Fig. 4.5. The reason for this is to show whether the implementation of local measures actually was well motivated. As expected, since all four local measures are formulated to be equal to 1 for a Poisson process just like the FF and CV, the local measures behave rather similar (compare Fig. 4.5). Note that the scaling of the y-axis is different in Fig. 4.5 and Fig. 4.6 and that the amplitude is much lower for the local measures (Fig. 4.6). Adding to this, the percentual difference in amplitude between the peaks and the valley is lower than that for the FF and CV. This means that the local measures actually are less sensitive to pronounced changes in firing rate than the global measures. The local measures are also able to detect the slow change of firing rate in the interval $(20, 40]$, in contrast to the FF. As expected all measures equals zero where the ISIs are of the same length.

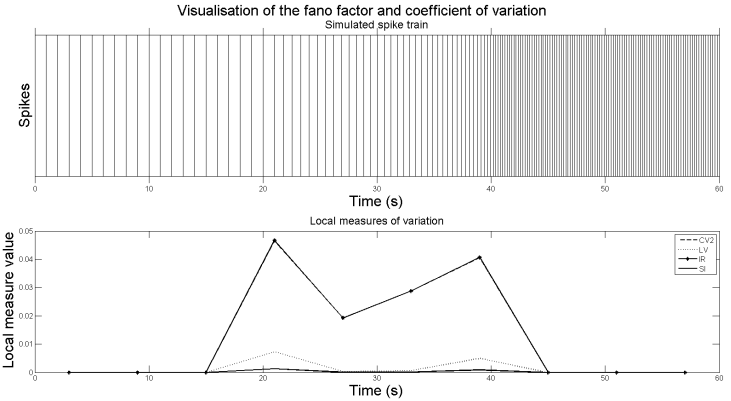

Figure 4.6: Visualisation of *local coefficient of variation* (CV_2), *local variation* (LV), *irregularity measure* (IR) and *spiking irregularity measure* (SI) (below) as local measures of a simulated recording (above). The recording is simulated with constant, low frequency $t = [0, 20]$, increasing frequency $t = (20, 40]$ and constant, high frequency $t = (40, 60]$.

The local measures have proven to be less sensitive to pronounced changes in firing rate [21]. But are they still able to measure the similarity between a given process and the homogeneous Poisson process?

Fig. 4.7 shows the local measures applied to a simulated recording with an underlying homogeneous Poisson process. It shows that CV_2 and LV are very close to 1 during the whole recording whereas IR and SI have values that are above and below 1 respectively. But, they are still rather close to 1 in comparison with e.g. the FF (see Fig. 4.4). Hence, they seem to be able to measure the similarity between a given process and the homogeneous Poisson process, while at the same time being less sensitive to sudden changes in firing rate.

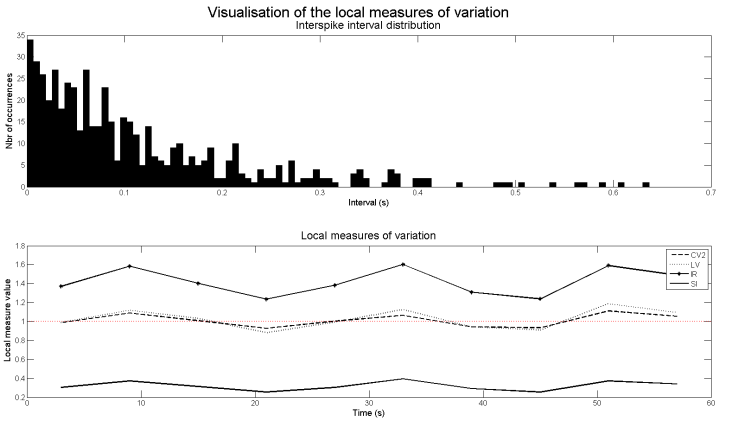

Figure 4.7: Visualisation of *local coefficient of variation* (CV_2), *local variation* (LV), *irregularity measure* (IR) and *spiking irregularity measure* (SI) (below) as local measures of a simulated recording with an underlying homogeneous Poisson process (above).

Irregularity Measures

Neuroscientists long believed that the use of information theory could enable a deeper understanding of the information processing of neural systems [22]. A possible issue with this belief is that the issues and goals of neuroscientists and communication engineers are very different: Communication engineers *design* systems while neuroscientists *analyse* existing systems. In spite of these differences, information-theoretic techniques has proven to provide useful insights in questions related to neuroscience [23].

Applying information measures to the data quantify the similarity, or dissimilarity, of the spike trains. Information measures can also, for this reason, be referred to as *irregularity measures*. In this work, two kinds of irregularity measures, both described below, are calculated: *entropy* and *spike train metrics*.

Entropy, the Direct Method The entropy is calculated for a certain ISI within a spike train. The spike train is defined by the time segment chosen from the data set. The definition of the entropy of an ISI, analogue to the one for a stimulus in [22], is given by:

Definition 2. *Let D be a discrete-valued ISI that assumes one of M values, $D \in \{\tau_1, \tau_2, ..., \tau_M\}$, and let $P[\tau_i]$ denote the probability with which each ISI within the segment occurs. The entropy of a certain ISI, $H(D)$, is defined as*

$$H(D) \triangleq -\sum_{i=1}^{M} P[\tau_i] \log_2 P[\tau_i]$$

In this implementation, $P[\tau_i]$ is approximated as the number of occurrences of that ISI within the segment divided by the total number of ISIs within the segment. The entropy equals zero when an ISI has unit probability, i.e., all ISIs within a segment are equal. It reaches its upper bound, $\log_2 M$, when all ISIs are equally likely, i.e., when all ISIs are different. This means that the entropy characterises ISI uncertainty. A larger value of entropy implies a greater uncertainty and larger variety of ISIs and vice versa.

Spike Train Metrics Spike train metrics are particularly useful for neural coding because they operate on time series of all-or-none events [25], recall that this is exactly what a series of action potentials are. The spike train metrics quantify the extent to which the patterns of two spike trains are dissimilar. The two metrics implemented, *spike time metrics* and *spike interval metrics*, are both *cost-based metrics*, meaning that a cost is assigned for the process of turning one spike train into another.

These spike train metrics are best suited for repeated trials, where similar spike trains are compared due to alignment of events. This

may not be the case in a single trial recording but the measures can still be useful with some adjustment. The costs of the both metrics are kept as they are defined but they are implemented on spike trains, or *groups*, within a segment. This means that the groups within a segment are compared, as opposed to different segments being compared to each other. After division of a segment into groups, each of these groups contain a specific number of spikes, n_m. The adjustment results in the metrics becoming measures of irregularity *within* a segment. If all groups of n_m spikes are similar each other the cost will be low and vice versa. Note that there is a cost for the number of spikes between groups being different (see below). With the adjustment made for single trial this cost will be equal to zero for comparisons between all groups in the segment except maybe for comparisons with the last group, which may contain less than n_m spikes due to the limited time interval that defines the segment.

Spike Time Metric: For the spike time metrics (TM), there are two kinds of costs defined for turning spike train A into spike train B:

1. the cost of deleting or inserting a spike is equal to 1.
2. the cost of moving a single spike in time, equal to $q|t_a - t_b|$, where t_a is the spike time for a spike in A, t_b the spike time for a spike in B and q a tunable weighing factor (in units of 1/sec).

For $q = 0$, the spike timing is irrelevant and the larger the q, the higher is the relative sensitivity of the metric to spike count and spike timing.

Spike Interval Metric: There are two costs for the spike interval metrics (IM), as well:

1. the cost of deleting or inserting a spike, equal to 1.
2. the cost of shortening or extending an ISI, equal to qt, where t is the amount that the interval has to be changed by and q a tunable weighing factor (in units of 1/s).

The parameter q has the same roll here as for the spike time metrics but note that changing the length of an interval, as in IM, is not the

same as moving a spike in time, as in TM. When an interval length is changed, the spike times of all following spikes are changed, whereas if a spike is moved in time it does not affect the following spikes.

Fig. 4.8 shows a visualisation of the irregularity measures entropy, TM and IM. Two simulated recordings has been used to illustrate how the measures behave. The first one (column 1) has constant firing rate, i.e. only one ISI interval, namely 0.5 seconds. The second (column 2) is drawn from a normal distribution. The plots show that a recording with evenly spaced spikes (first recording) has low irregularity and results in lower values whereas a signal with many different ISIs (second recording) has high irregularity and results in higher values of irregularity. Note that the scale for the entropy and the spike train metrics are different. In this context a value of 12 for the entropy is high while very low for the spike train metrics.

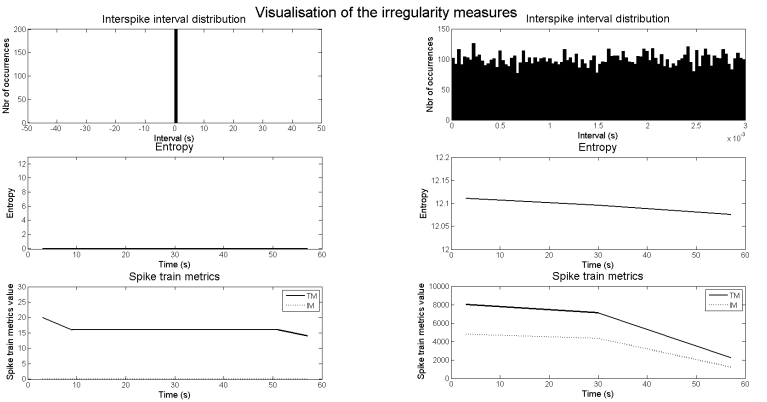

Figure 4.8: Visualisation of the irregularity measures *entropy* (middle), *spike time metric* (TM) and *spike interval metric* (IM) (below) as measures of two simulated recordings (above). First recording (left) was simulated with constant firing rate, the second (right) with an underlying normal distribution.

Statistical Significance

The features presented above are meant to be descriptive: In this thesis work the hypothesis is that they can be used to describe differ-

ent states, especially differ the baseline from the post levodopa state. To decide whether the features can be used to differentiate between two states one can investigate whether the difference between feature values in two different states is *statistically significant*. If the difference between feature values in the two states are statistically significant it means that one, with some degree of confidence, can state that they belong to two different distributions [26].

To decide whether the difference between feature values in the baseline and post levodopa state were statistically significant a paired t-test were used. The paired t-test used tests the null hypothesis H_0 that two samples, X and Y, come from distributions with equal means. The difference $X - Y$ is assumed to come from a normal distribution with unknown variance and the level of confidence used was 95%. To perform the paired t-test, MATLAB's function `ttest` was used.

Feature Vector Extraction

The features presented above, see Table 4.1 for an overview, were calculated for every segment of the recordingss. More specifically, for every segment, all feature values were gathered to form a *feature vector*. The collection of feature vectors, i.e. the feature vectors gathered from all segments, allows one to investigate how the feature values propagate over time.

The hope is that one or several features change over time as the behaviour or actions of the animals changes. If the feature values exhibit changes that in some way are connected to changes of the behaviour or actions of the animal, one may be able to *classify*, or connect the *clusters* formed, to different states. These states could, as have been mentioned before, be e.g. start, slowing and stop of locomotion or the diseased dyskinetic state. At least, these states are the ones investigated in this thesis work.

Feature	Description	Notation
1	Average rate	$<r>$
2	Variance of rate	σ_r^2
3	Average number of spikes	$<n>$
4	Variance of number of spikes	σ_n^2
5	Fano factor	FF
6	Coefficient of variation	CV
7	Average local coefficient of variation	$<CV_2>$
8	Variance of local coefficient of variation	$\sigma_{CV_2}^2$
9	Average local variation	$<LV>$
10	Variance of local variation	σ_{LV}^2
11	Average irregularity measure	$<IR>$
12	Variance of irregularity measure	σ_{IR}^2
13	Average spiking irregularity measure	$<SI>$
14	Variance of spiking irregularity measure	σ_{SI}^2
15	Entropy	H
16	Spike time metric	TM
17	Spike interval metric	IM

Table 4.1: Table over features used for clustering and classification.

4.4 Dimensionality Reduction

The use of all 17 features stated in Table 4.1 presents one with a 17 dimensional space to use for clustering or classification. To investigate whether the dimensionality of the problem could be reduced, one can make use of, e.g., *principal component analysis* (PCA) [26]. Generally, component analysis is an unsupervised approach to find which features that define a d-dimensional feature space. Principal component analysis projects the d-dimensional feature data onto a new orthogonal d-dimensional space, creating linear combinations of the original

features. This is done by using a projection matrix $\boldsymbol{P}$:

$$\boldsymbol{F}\boldsymbol{P} = \boldsymbol{F}_P,$$

where $\boldsymbol{F}$ is the $[n \text{ x } d]$ dimensional matrix (n being the number of observations) containing the original feature data, $\boldsymbol{P}$ the $[d \text{ x } d]$ dimensional projection matrix and $\boldsymbol{F}_P$ the $[n \text{ x } d]$ dimensional matrix holding the feature data projected onto the new space.

The projection matrix $\boldsymbol{P}$ is constructed so that the projected data $\boldsymbol{F}_P$ has columns with decreasing variance. This means that the first column covers the largest amount of the variance in the original space, the second the second largest amount and so on. Hence, all columns of $\boldsymbol{F}_P$ covers the entire original space variance. This means that projection onto the principal component space does not reduce the dimensionality: No information in the original data is lost. If one wishes to reduce the dimensionality to dimension p, one simply keeps the first p columns in $\boldsymbol{F}_P$ and let them represent the original data. This reduces the dimensionality while keeping the largest amount possible of the original data's variance.

A two-dimensional projection example, where the projection simply is a rotation, can be found in Fig. 4.9 where each data point (red) is defined by two features and the principal components are marked by two arrows (blue and black). If one wishes to reduce the dimensionality it is preferable to choose the black principal component to represent the data in the principal component space as the largest variance is found along its direction.

PCA was performed using MATLABs built in function `pca`. The following parameters, returned from `pca`, were used:

- **the principal component coefficients**: the matrix used to project the original feature data onto the principal component space, i.e. $\boldsymbol{P}$.
- **the principal component score**: the representation of the features in the principal component space, i.e. the projected data $\boldsymbol{F}_P$.

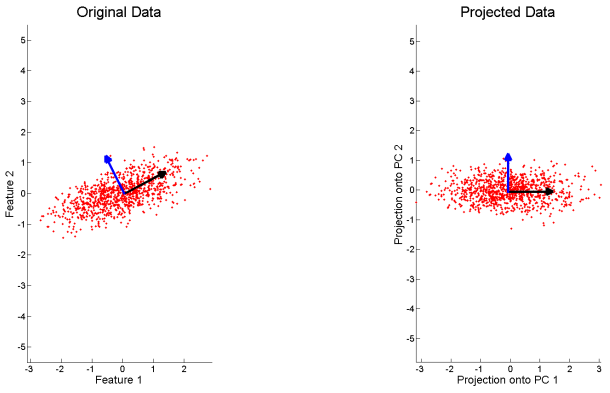

Figure 4.9: Visualisation of a two-dimensional principal component analysis example with the original data (left) and the data projected onto the new principal component space (right).

- **the principal component variances**: the amount of variance preserved when projecting the features space into the principal component space.

Based on PCA, two reduced feature spaces were created. The first approach to create a reduced feature space, the *reduced principal component space*, was to make use of the principal component variances. These were used to decide the dimension, p, of the new reduced space, i.e. the number of colums in $\boldsymbol{F}_P$ that had to be kept to cover 90% and 99% of the original feature space variance. Subsequently, the clustering and classification were performed on the p_{90} and p_{99} first columns.

The second approach, creating the *reduced feature space*, was based on the weights in the principal component coefficient matrix. The dimension were, as in the first approach, decided by the principal component variances (p_{90} and p_{99}). That number of original features were used for the new space according to the following procedure:

1. The feature with the largest weight in column one of $\boldsymbol{P}$ is chosen for the reduced feature space.

2. The feature with the largest weight in column two of $\boldsymbol{P}$ is chosen, if this feature is the same as the one chosen in step 1., the feature with the next largest weight is chosen.

3. The feature with the largest weight in column three of $\boldsymbol{P}$ is chosen. If this is the same feature as either the one chosen in 1. or in 2., the feature with the next largest weight is chosen. If that feature also is the same as one of those chosen in 1. or 2., the feature with the third largest weight is chosen.

4. This procedure is continued until p_{90} and p_{99} number of original feature has been chosen.

The reduced number of original features was subsequently used to perform clustering and classification.

4.5 Clustering: Unsupervised Learning

Clustering allows for categorisation of the segments into states without having any prior knowledge as to what state is actually "correct" [26]. Hence, the process of clustering is exploratory and may offer some previously unknown facts about the nature or structure of the data.

The aim of clustering is to partition the data of n *samples*, the segments, into c *clusters*, the states. Samples within the same cluster should be alike in some way while they should differ from samples within other clusters. To create clusters one may start with $c = n$ number of clusters, where each cluster contains only one sample and then step by step merge these to form new clusters. This type of clustering is called *hierarchical clustering*.

Hierarchical Clustering

The process of hierarchical clustering starts, as stated above, with every sample being declared one cluster each. After this, two samples are merged to form a new cluster. This merge results in the new number of clusters becoming $c = n - 1$. Which samples that should be merged is decided by some similarity measure, e.g. shortest Euclidean distance between feature vectors. After this, either a sample is merged with the

previously newly formed cluster or with another sample to form yet another new cluster, and the total number of clusters are $c = n - 2$. Continuing this process finally results in all clusters becoming one, containing the whole data set. This process is illustrated by Fig. 4.10 below, where a distance criteria has been used to form clusters.

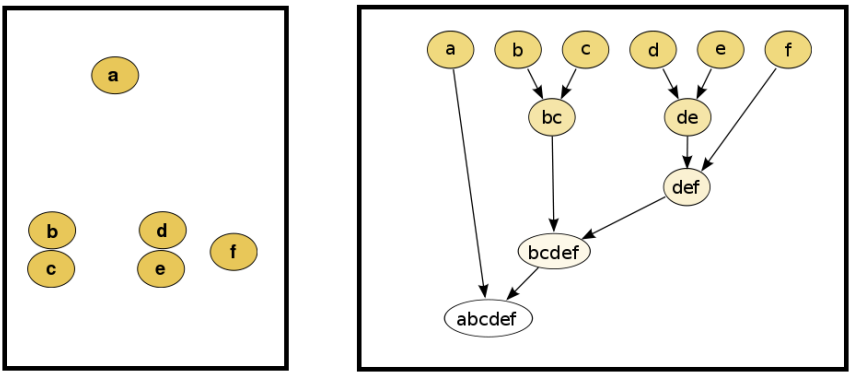

Figure 4.10: Illustration of the process of hierarchical clustering of a data set (left) with a distance criteria to form clusters (right) [27, 28].

Depending on how many clusters that is of interest, the process can be stopped at that number. Another reason to stop the merging of clusters could be that the two clusters about to be merged does not have values similar enough to form a new cluster. Similarity could e.g. be measured in the distance between the clusters.

After performing clustering, the clustering quality can be measured. The ultimate goal is that each cluster is well separated from the others and that the dispersion within each cluster is small. This is not always possible due to the structure of the data to be clustered. A data set containing only identical, or very similar, samples will never result in clusters that are well separated and a data set with very different samples will never have a low dispersion.

A simple way to measure the clustering quality is to calculate the percentage of segments that has been correctly clustered. Since clus-

tering is a blind process, i.e. there is no prior knowledge about what segments belong to which cluster, it is not known what *correctly clustered* is. Since, in this work, the aim is to separate states from each other, the labelling of clusters are not really important and the true clusters can be chosen so that the percentage is maximised. As an example, if two clusters are used, there will be one percentage of segments correctly clustered if the baseline is labelled *1* and the post levodopa state *2*, and another vice versa. Another way to measure the clustering quality is by help of *criterion functions*.

Criterion Functions

Criterion functions are generally used to optimise the quality of the clustering, i.e., to *find* the partition of the data that optimises them [26]. But, if the partition has already been made they can be used to measure the quality of the clustering. The criterion functions used in this work are presented below.

The Sum-of-Squared-Error Criterion The sum-of-squared-error criterion is the most widely used criterion function [26]. It measures the dispersion within a cluster by comparing each sample of a cluster to the mean centre. One wishes low values for the sum-of-squared-error, since this means that the samples within the cluster with that corresponding error are much *alike* each other.

The sum-of-squared errors is defined by

$$J_e = \sum_{i=1}^{c} \sum_{\boldsymbol{x} \in D_i} ||\boldsymbol{x} - \boldsymbol{m}_i||^2$$

where c is the total number of clusters, D_i is the notation of the ith cluster, $\boldsymbol{x}$ denotes a sample and $\boldsymbol{m}_i$ the sample mean within the ith cluster. Note that the boldface characters denotes that $\boldsymbol{m}_i$ and $\boldsymbol{x}$ are vectors. In this case, more specifically, $\boldsymbol{x}$ is a feature vector and $\boldsymbol{m}_i$ the mean over all feature vectors in the ith cluster. The Euclidean distance is used as distance function.

The Between-Cluster Criterion The between-cluster criterion is a nice complement to the sum-of-squared-error criterion. It does not measure the scattering within a cluster, but the scattering between

clusters. High values of between-cluster scattering is preferable, since this means that the clusters are well separated, i.e. that the samples in different clusters are much *unlike* each other.

The between-cluster criterion is based on the between-cluster-scatter matrix $\boldsymbol{S}_B$,

$$\boldsymbol{S}_B = \sum_{i=1}^{c} n_i(\boldsymbol{m}_i - \boldsymbol{m})(\boldsymbol{m}_i - \boldsymbol{m})^t$$

where n_i is the number of samples in the ith cluster, $\boldsymbol{m}$ the mean of all samples in the data set and t denotes the transpose. The between-cluster-criterion is simply the trace of the between-cluster-scatter-matrix $\boldsymbol{S}_B$.

$$J_b = \mathrm{tr}[\boldsymbol{S}_B] = \sum_{i=1}^{c} n_i||\boldsymbol{m}_i - \boldsymbol{m}||^2.$$

Note that the boldface characters denotes vectors here as well. As for the between-cluster criterion, $\boldsymbol{m}_i$ is the mean over all feature vectors in the ith cluster and here, $\boldsymbol{m}$ is the mean over all feature vectors in all clusters.

4.6 Classification: Supervised Learning

During classification each feature vector is used to assign every *object* to a *group* [26]. In this case an object is a segment of time and a group, or class, corresponds to a state.

During classification a class is assigned to each object previous to the classification. In this case it means that *a priori* knowledge about when the animal is in a certain state of behaviour is needed to perform the classification. Hence, the task of classification is not to find out what class a certain segment belongs to, but to minimise the cost of dividing all segments into the previously decided classes. The difficulty of this task is decided by the variability of the feature values for segments belonging to the *same* class relative to the difference between feature values in *different* classes. The division of segments into different classes is done by using the feature values. Segments with feature

values that are alike should be grouped into the same class and there should be a distinct difference in feature values between the segments grouped into different classes. The process of grouping the segments into classes can accessibly be visualised by the use of a *decision tree*.

Decision Trees

A decision tree is characterised by a series of questions that have two or several possible answers [26]. Depending on the answer, a new question is asked until either sufficiently many questions has been answered to decide what class a certain object belongs to or the process is stopped due to some condition set beforehand. The name *decision tree* comes from that the answer to each question is followed by a split of the whole data set or a data subset. An example of a decision tree is displayed in Fig. 4.11.

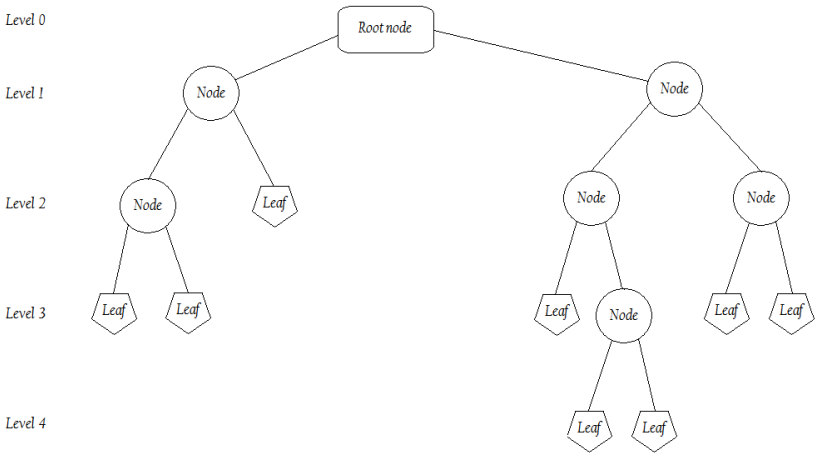

Figure 4.11: Basic decision tree with 4 levels where the classification process proceeds from top to bottom.

The creation of a decision tree starts with a base called the *root node*, which holds all time segments. In our case a simple yes/no question is asked, namely if a certain feature value is larger or smaller than the value that most significantly divides the segments into two different states. The outcome is that the data is divided into two groups for which two new questions can be asked to make further divisions. Each

such division creates a new *node*, holding a subset of the data, and if the node is pure enough it is declared a *leaf*. When the process of classification reaches a leaf, that trail of divisions is complete. The leaf furthest from the root node decides how many *levels* the classification consists of, with level 0 being the root node. The number of levels is equal to the number of splits that has been performed to create the subset in the leaf furthest from the root node. The declaration of a leaf is where the question of "when to stop splitting" comes into light. If a very accurate classification is wanted, with the extreme case being that all segments are correctly classified. In some cases, this can lead to a very large number of splits which may require a lot of calculations. Continuing to split the decision tree like this also introduces another problem: *overfitting*.

Overfitting a Decision Tree An optimal setup to perform a classification would be to have access to a large amount of the same type of data gathered in different trials, i.e. many repeated trials. One part of the data would then be used to train the classifier and the other part of the data to evaluate the performance of the classifier and validate the result. Unfortunately, a sufficient amount of datasets is not always available for training and validation on separate datasets, as is the case in this thesis work. A solution is to train and evaluate the classifier on the same data set, but this can result in an overfitting of the decision tree. Overfitting means that the classifier is overly adapted to a certain data set, which will allow for very successful results when performing classification on the same data set. To a certain degree, this can be avoided by dividing the data and using *cross-validation*.

The cross-validation used in this thesis work is the *m-fold cross-validation*, more specifically a 10-fold cross-validation. During a m-fold cross-validation the dataset is randomly split in m disjoint sets of equal size n/m, where n is the total number of segments. After this partition, the classifier is trained m times, one time with each of the data sets as the validation set and all other sets as training sets.

4.7 Computation Scheme for Clustering and Classification

Dyskinesia Recording 4 and 8, recorded at NRC, were used to perform clustering and classification of each neuron separately. The following versions of the feature space, with the data 30 or 5 min post injection removed, were used to identify the baseline and the post levodopa state:

- *Full feature space*, i.e. the space based on all features.
- *Reduced principal component space*, covering 90% and 99% of the original feature space.
- *Reduced feature space*, with one and two original features respectively.

The classification was performed twice using MATLAB's function `fitctree` with 10-fold cross-validation and two or trhee true classes respectively. When two classes were used, one class denoted the baseline, i.e. the time segments before the injection. The other class denoted the segments after the injection. For the data where only 5 min post injection were removed, three classes were used: the third class denoted the *transition state*, between 5 and 30 min post injection.

For clustering, the scattering measures were calculated for 1 up to 15 clusters. Based on the progression of these measure values the clustering were finally performed, using MATLAB's function `cluster`, for 2 and 3 clusters.

Performance Evaluation

The clustering quality for each neuron was measured by the fraction of "correctly" clustered segments. A segment was assumed to be correctly clustered if it was clustered according to the cluster label combination that maximises the total fraction of correctly clustered segments. More specifically this means that for, e.g., 2 states, 2 fractions were calculated:

1. The fraction of correctly clustered segments if the baseline was labelled "1" and the post levodopa state "2".

2. The fraction of correctly clustered segments if the baseline was labelled "2" and the post levodopa "1".

The labelling with the largest fraction of correctly clustered segments over the whole recording was then used to decide whether a segment was correctly clustered or not. For the classification, the performance was also measured by the fraction of correctly classified segments. Here, however, there is no question of what "correct" is because the classification is performed based on the key holding the correct labels for each segment.

5

Results

5.1 Feature Extraction

The results presented for the feature extraction are based on values obtained from Dyskinesia Recording 4 and 7. They illustrate whether the features are able tp differentiate between different states, in this case the baseline from the post levodopa state. First there will be one box plot for each feature, Figs. 5.1 - 5.9, showing feature values before and after injection of levodopa. More specifically, there are for each neuron in the recording, two boxes: the first one includes all feature values from the segments *before* the injection of levodopa and the second all feature values from the segments *after* the injection.

The boxes are separated by the median, the upper (brown) part is the 25th percentile and the lower (gray) part the 75th percentile. The error bars' upper and lower limits represent the maximum and minimum, respectively.

Following the box plots for each feature Tables 5.1 and 5.2 states how large percentage of the neurons that exhibits a significant change in feature values after the injection of levodopa. This result is presented both for Dyskinesia Recording 4 and 7 and serves as a summary of the results for the feature extraction.

The Rate and Spike Count

In Figs. 5.1 and 5.2, visualisations of the rate and the spike count are presented. The results for the rate and spike count average, Figs. 5.1a and 5.2a, are closely related, as are the results for the rate and spike

count variance, Figs. 5.1b and 5.2b: The rate is simply a scaled version of the spike count. Because of this close relation their results will be presented together.

Note that there is a significant change in feature values (well separated boxes) post levodopa injection for some neurons in Figs. 5.1a and 5.2a, e.g. the second *RFA; Left* and *GP; Left*, while others do not seem to exhibit any significant change, e.g. *SNr; Left*. For the rate and spike count variance (Figs. 5.1b and 5.2b) the large variance of e.g. the first *DMS; Left; post* and *SNr; Left; pre* overshadows the results from the other neurons. However, the results in Table 5.1 show that 80% of all neurons exhibit a significant change in rate and spike count variance after the injection of levodopa.

Some of the neurons have increased feature values after the injection, e.g. the second *RFA; Left* in Fig. 5.1a, while other have decreased, e.g. the second *GP; Left* in the same figure. Note that this variation exists for all four features and both the left (healthy) and right (lesioned) hemisphere as well as within the same site: For example *RFA; Left* in Fig. 5.1a has one neuron that has decreased feature values post levodopa injection and one that has increased feature values post levodopa injection.

The Global Measures of Variability

Note that some of the neurons, e.g. the first *DMS; Left*, exhibit a significant change in feature values (well separated boxes) post levodopa injection whereas others does not exhibit any noteable change, e.g. the last *DLS; Right*. Also note that some neurons have increased feature values after the injection, e.g. the first *RFA; Left* and *DMS; Left*, while others have decreased, e.g. the second *DMS; Left* and *DLS; Right*. This variation exists within both the left (healthy) and right (lesioned) hemisphere as well as at the same site: For example *DMS; Left* has one neurons with increased and another with decreased feature values after the injection of levodopa.

As for the rate and spike count variance, there are some neurons that overshadows the results of the others, making it hard to distinguish whether the Fano factor and the coefficient of variation well

separates the baseline from the post levodopa state. Table 5.1 shows that 47% percent of all neurons exhibit a significant change in Fano factor after injection and 73% a significant change in coefficient of variation.

The Local Measures of Variability

In Fig. 5.4 - 5.7, visualisations of the local measures of variation: the average and variance of the local coefficient of variation, the local variation, the local irregularity measure and the local spiking irregularity measure, are presented. Because of the measures close relation mathematically the results for the local measures of variability averages will be presented together as well as the local measures of variability variances.

Note that, as for the previously presented feature results, there are neurons that exhibit significant changes in feature values (well separated boxes) for the averages, e.g. the first *DMS; Left* whereas there are other neurons that do not. Also notice that there is a larger difference pre and post injection for the first *DMS; Left* in the $< IR >$ and $< SI >$, Fig. 5.6a and 5.7a, than for the $< CV_2 >$ and $< LV >$, Fig. 5.4a and 5.5a. Even though the features are closely related they do not perform equally in differentiating the baseline from the post levodopa state: As can be seen in Table 5.1, the $< LV >$ and $< SI >$ have 80% of the neurons exhibiting a significant change post levodopa injection while the $< CV_2 >$ and $< IR >$ only have 67%.

Also note that generally, the local measures of variability do not have as many neurons exhibiting a significant change in values pre and post levodopa as the rate and spike count, i.e. there are not as many well separated boxes for the local measure of variability. This is also confirmed by the percentages presented in Table 5.1, where they are generally lower for the local measures of variability.

Some of the neurons have an increase in feature values post injection while others have a decrease: This is, as for the previously presented features, a variation that exists both within the left (healthy) and right (lesioned) hemisphere as well as at the same site.

Again, the variance of these features Figs. 5.4b - 5.7b have neurons that overshadows the results from the others, e.g. *DMS; Left* and *DLS; Right*. In Table 5.1, however, it is obvious that the variance of these measures have a lower performance than the average does: $\sigma^2_{CV_2}$ have a percentage of 67% all neurons exhibiting a significant change post levodopa injection and the others have a percentage of 73%.

The Irregularity Measures

In Figs. 5.9 and 5.8, visualisations of the irregularity measures: the entropy and spike train metrics (spike time metric and spike interval metric), are presented. Note that, compared to the previous features, there are no neurons that, to the same extent, overshadows the results of the others. Also note that, for the spike train metrics in Fig. 5.8, there are some neurons that have decreased values post levodopa injection while others have increased. This, however is not the case for the entropy, Fig. 5.9, where all neurons exhibit an increase in feature value post levodopa injection. But, when investigating the post levodopa change of entropy for Dyskinesia Recording 7, the same result was not found. Due to the larger number of neurons (106) in this recording, this result is simply stated and not visualised like the box plot in Fig. 5.9.

The entropy for Dyskinesia Recording 4, Fig. 5.9, also has a larger number of well separated boxes than the other features, e.g. more neurons exhibiting a significant change post levodopa injection. The spike train metrics have some neurons exhibiting very significant changes post levodopa injections while others do not. This is also mirrored in Table 5.1 where the entropy has a percentage as high as 93% and the spike train metrics have 80% and 87% respectively.

Because of the small variance in feature values in the right (lesioned) hemisphere, Fig. 5.8, it is hard to distinguish whether there are both increases and decreases of feature values post levodopa, but this variation obviously exists within the left (healthy) hemisphere and at the same site, e.g. *RFA; Left* in Fig. 5.8a.

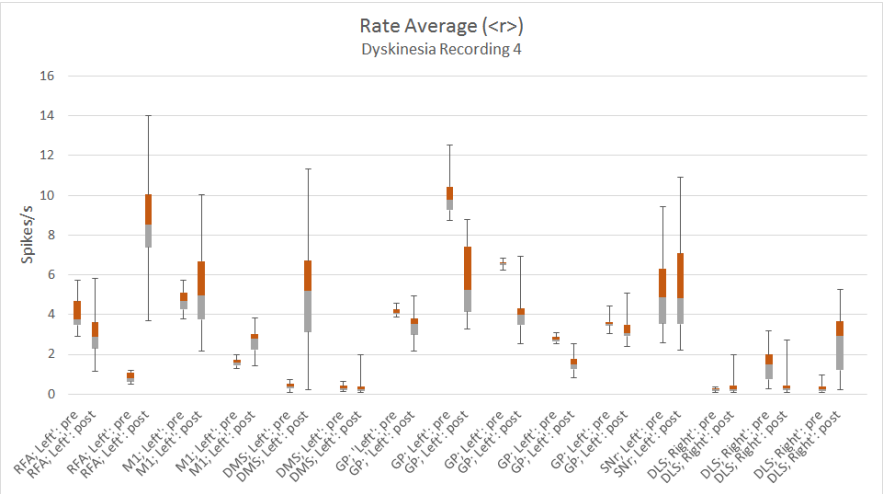

(a)

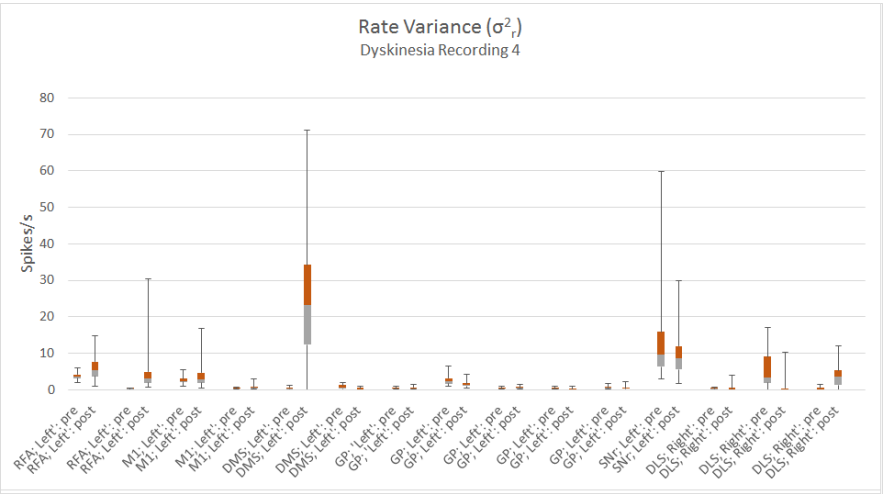

(b)

Figure 5.1: The rate average **(a)** and variance **(b)** pre and post levodopa injection for all 15 neurons of Dyskinesia Recording 4. Neurons from the left hemisphere on the far left: (RFA) Rostral Forelimb Area, (M1) Primary Motor Cortex, (DMS) Dorsomedial Striatum, (GP) Globus Pallidus and (SNr) Substantia Nigra and neurons from the right to the far right: (DLS) Dorsolateral Striatum.

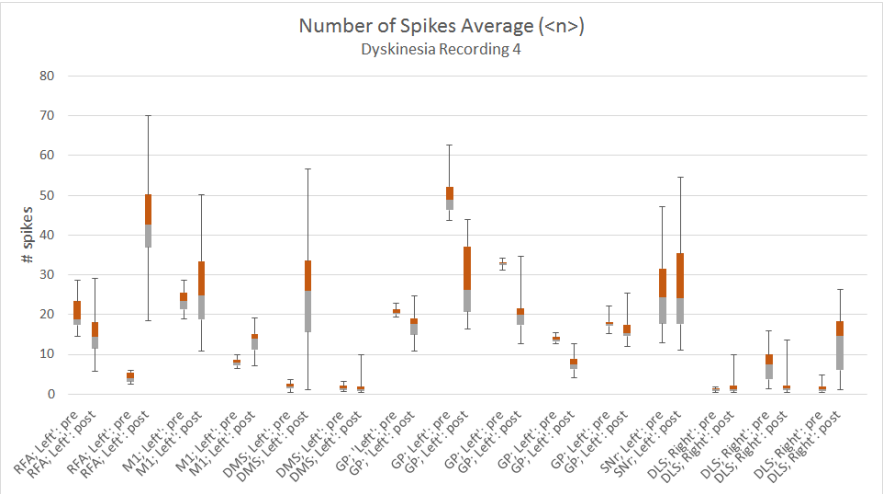

(a)

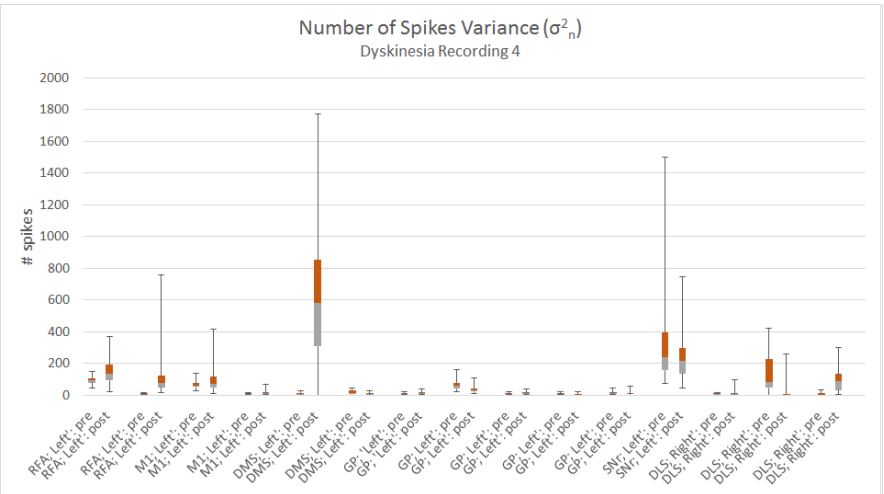

(b)

Figure 5.2: Number of spikes average **(a)** and variance **(b)** pre and post levodopa injection for the neurons of Dyskinesia Recording 4. Neurons from the left hemisphere on the far left: (RFA) Rostral Forelimb Area, (M1) Primary Motor Cortex, (DMS) Dorsomedial Striatum, (GP) Globus Pallidus and (SNr) Substantia Nigra and neurons from the right to the far right: (DLS) Dorsolateral Striatum.

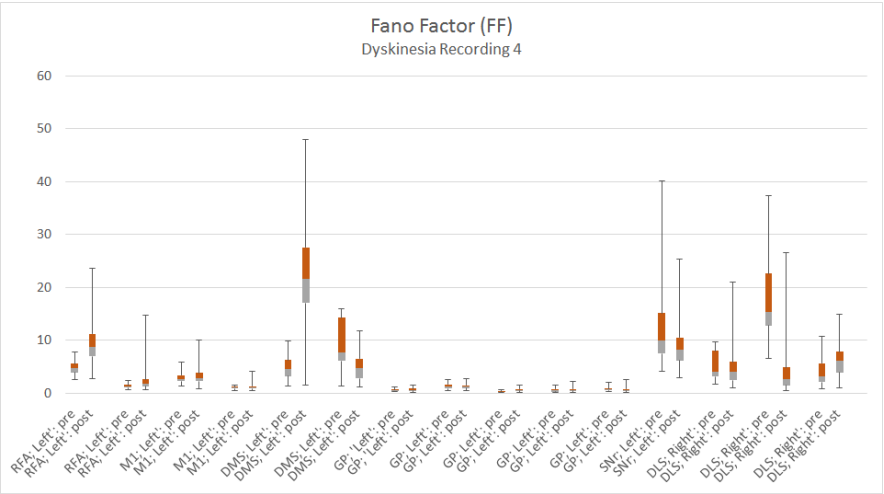

(a)

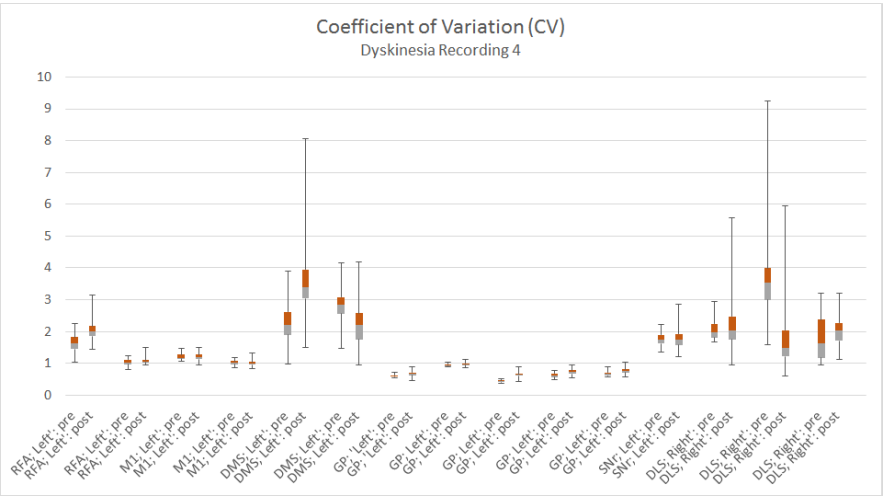

(b)

Figure 5.3: The Fano factor **(a)** and coefficient of variation **(b)** pre and post levodopa injection for the neurons of Dyskinesia Recording 4. Neurons from the left hemisphere on the far left: (RFA) Rostral Forelimb Area, (M1) Primary Motor Cortex, (DMS) Dorsomedial Striatum, (GP) Globus Pallidus and (SNr) Substantia Nigra and neurons from the right to the far right: (DLS) Dorsolateral Striatum.

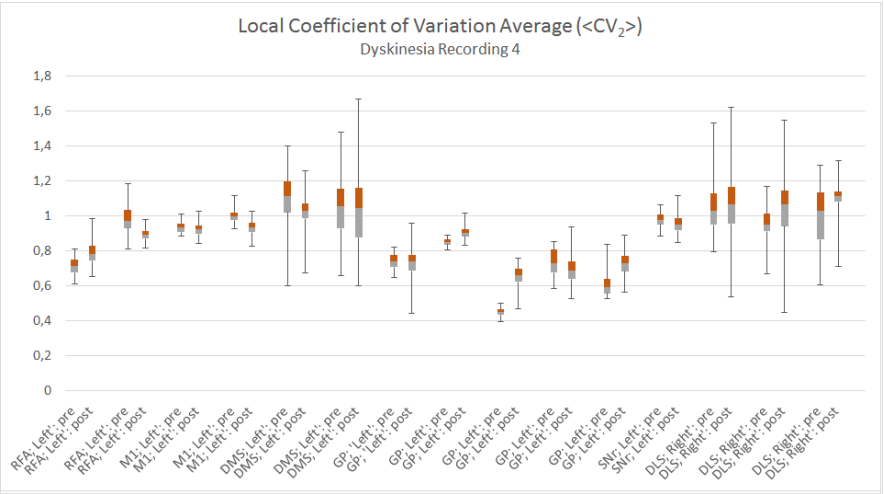

(a)

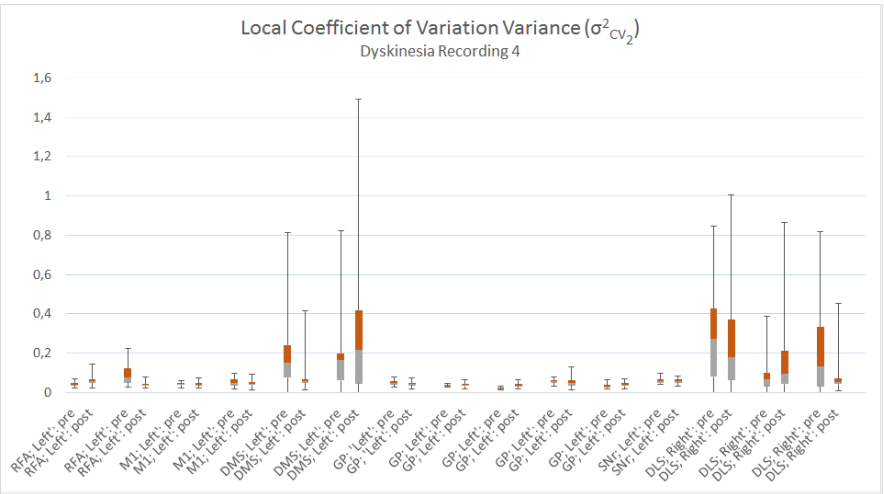

(b)

Figure 5.4: The local coefficient of variation average **(a)** and variance **(b)** pre and post levodopa injection for the neurons of Dyskinesia Recording 4. Neurons from the left hemisphere on the far left: (RFA) Rostral Forelimb Area, (M1) Primary Motor Cortex, (DMS) Dorsomedial Striatum, (GP) Globus Pallidus and (SNr) Substantia Nigra and neurons from the right to the far right: (DLS) Dorsolateral Striatum.

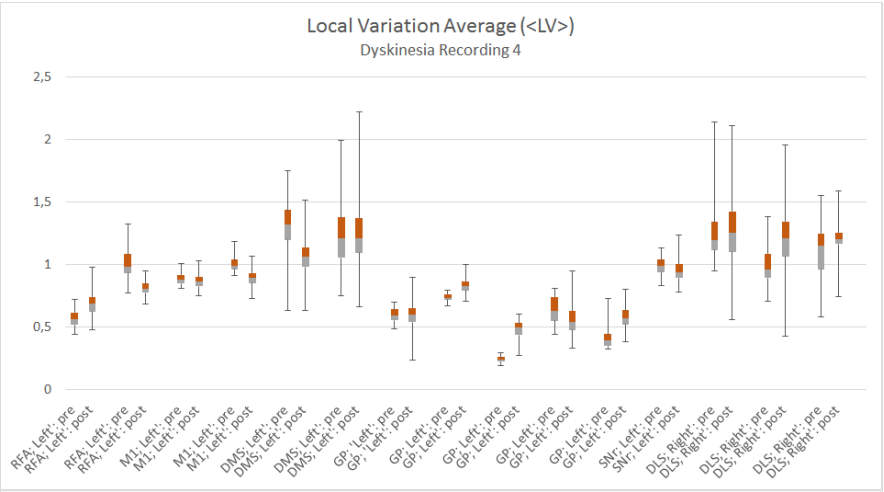

(a)

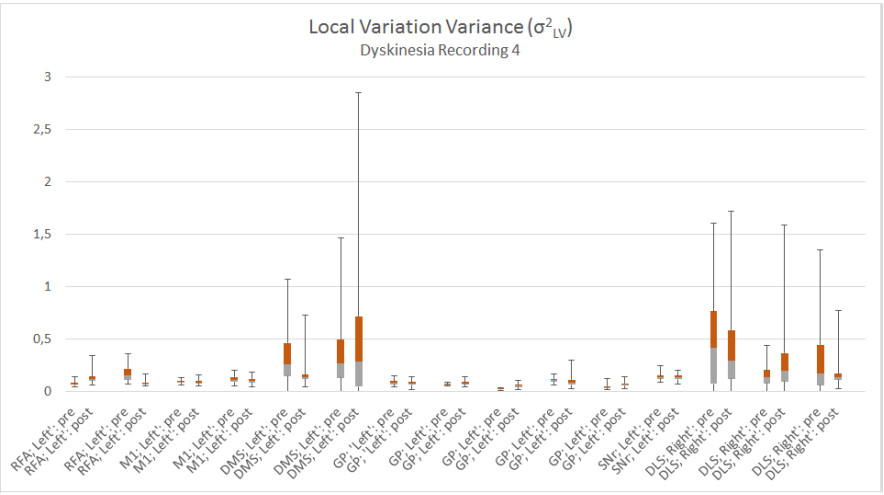

(b)

Figure 5.5: The local variation average **(a)** and variance **(b)** pre and post levodopa injection for the neurons of Dyskinesia Recording 4. Neurons from the left hemisphere on the far left: (RFA) Rostral Forelimb Area, (M1) Primary Motor Cortex, (DMS) Dorsomedial Striatum, (GP) Globus Pallidus and (SNr) Substantia Nigra and neurons from the right to the far right: (DLS) Dorsolateral Striatum.

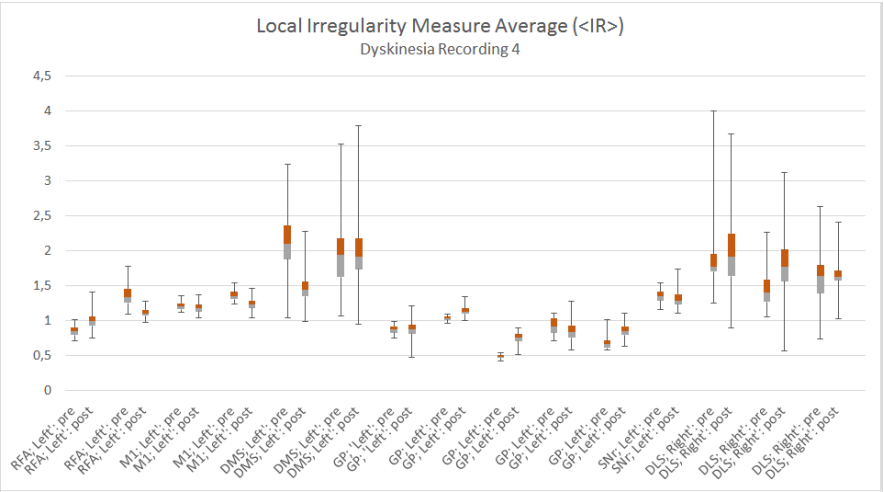

(a)

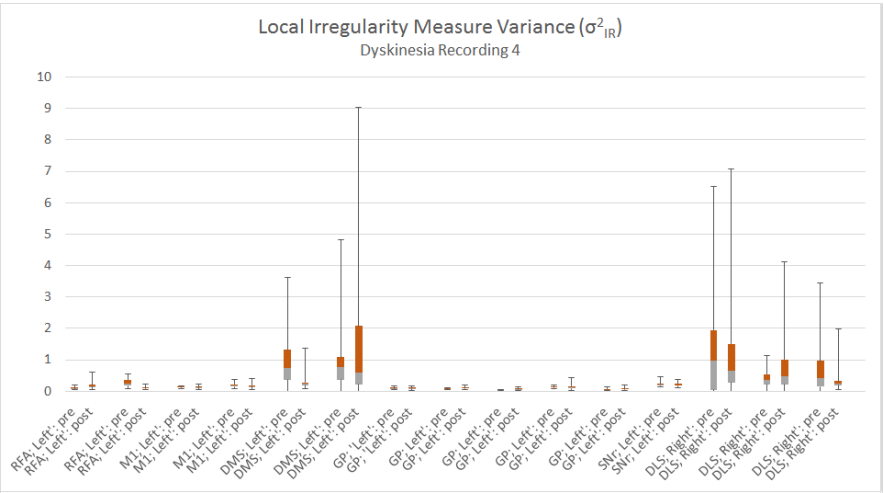

(b)

Figure 5.6: The local irregularity measure average **(a)** and variance **(b)** pre and post levodopa injection for the neurons of Dyskinesia Recording 4. Neurons from the left hemisphere on the far left: (RFA) Rostral Forelimb Area, (M1) Primary Motor Cortex, (DMS) Dorsomedial Striatum, (GP) Globus Pallidus and (SNr) Substantia Nigra and neurons from the right to the far right: (DLS) Dorsolateral Striatum.

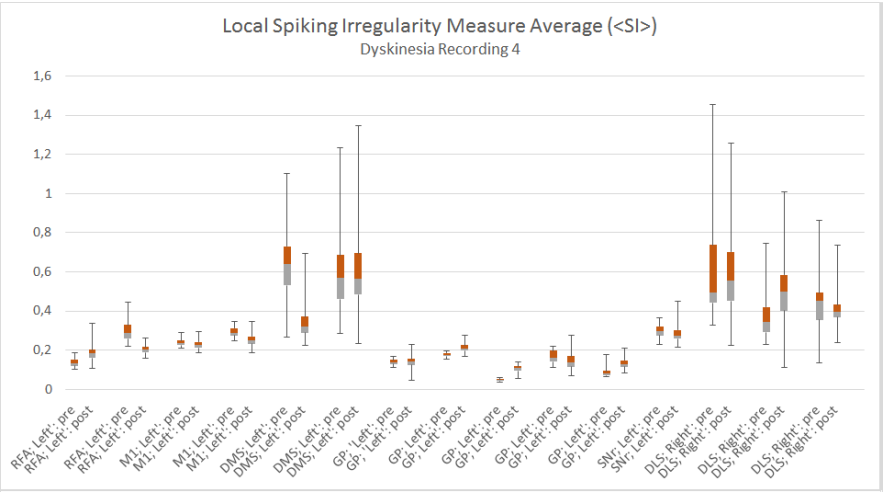

(a)

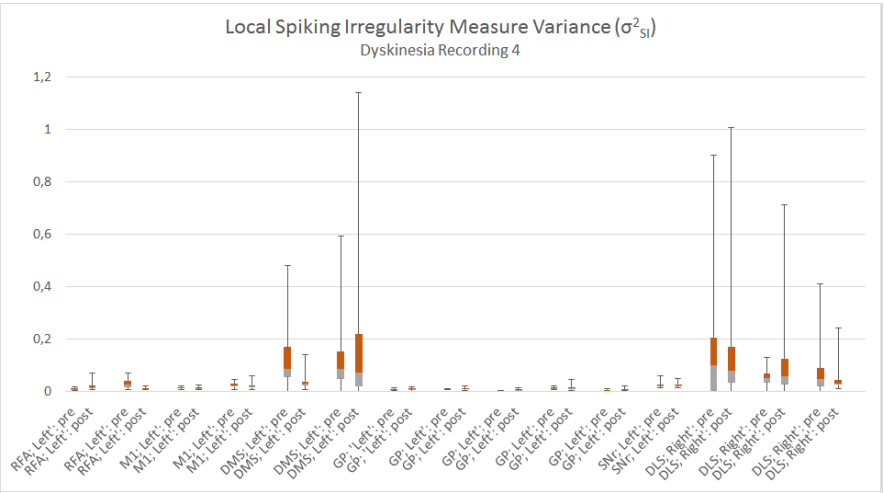

(b)

Figure 5.7: The local spiking irregularity measure average **(a)** and variance **(b)** pre and post levodopa injection for the neurons of Dyskinesia Recording 4. Neurons from the left hemisphere on the far left: (RFA) Rostral Forelimb Area, (M1) Primary Motor Cortex, (DMS) Dorsomedial Striatum, (GP) Globus Pallidus and (SNr) Substantia Nigra and neurons from the right to the far right: (DLS) Dorsolateral Striatum.

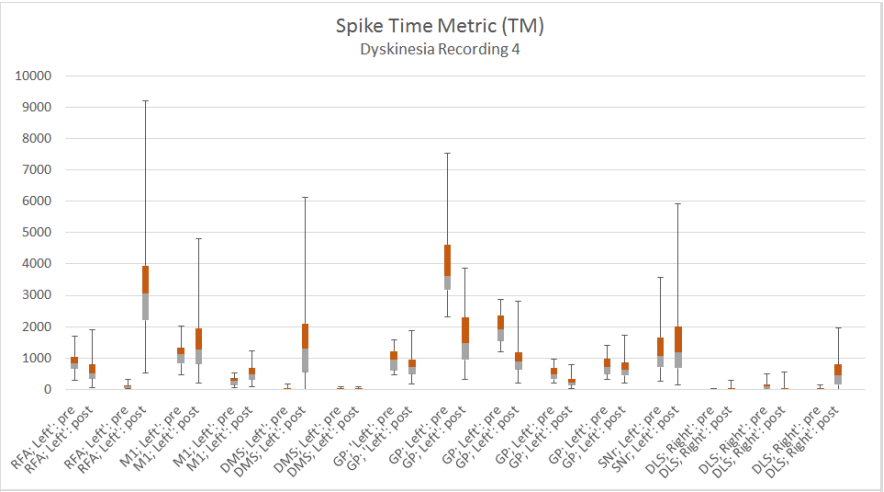

(a)

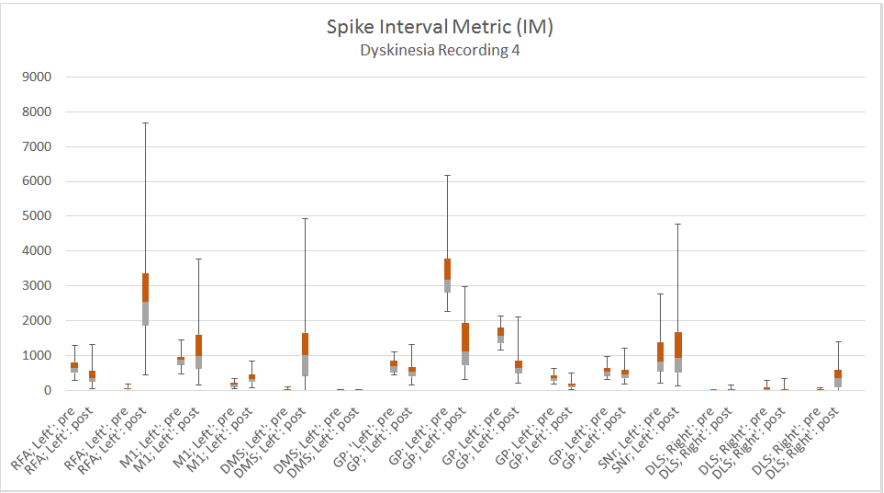

(b)

Figure 5.8: The spike train metrics: spike time metric **(a)** and spike interval metric **(b)** pre and post levodopa injection for the neurons of Dyskinesia Recording 4. Neurons from the left hemisphere on the far left: (RFA) Rostral Forelimb Area, (M1) Primary Motor Cortex, (DMS) Dorsomedial Striatum, (GP) Globus Pallidus and (SNr) Substantia Nigra and neurons from the right to the far right: (DLS) Dorsolateral Striatum.

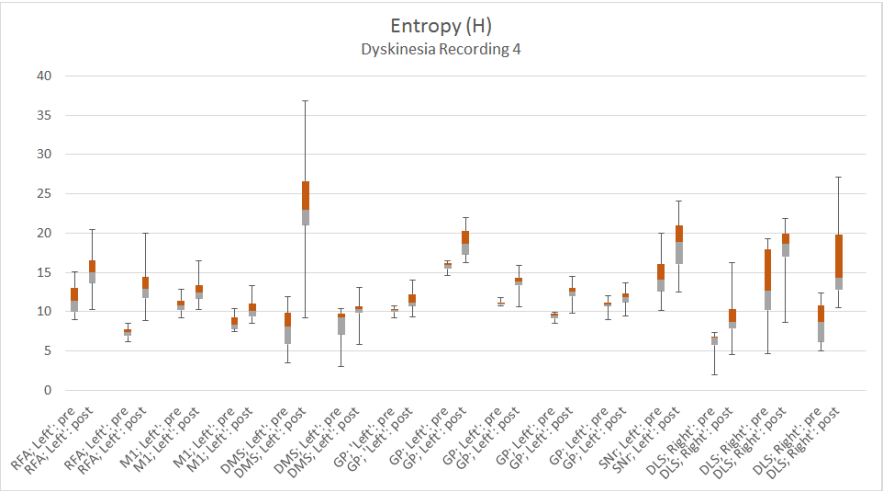

Figure 5.9: The entropy pre and post levodopa injection for the neurons of Dyskinesia Recording 4. Neurons from the left hemisphere on the far left: (RFA) Rostral Forelimb Area, (M1) Primary Motor Cortex, (DMS) Dorsomedial Striatum, (GP) Globus Pallidus and (SNr) Substantia Nigra and neurons from the right to the far right: (DLS) Dorsolateral Striatum.

Summary of the Feature Extraction Results

Table 5.1 and 5.2 offers a summary of the feature extraction results, showing the percentage of all neurons, neurons in the left (healthy) hemisphere and the right (lesioned) hemisphere that exhibit a significant change in feature values post levodopa injection.

Note that the values of 100% for the right hemisphere of Dyskinesia Recording 4, Table 5.1, are based on three neurons alone. This amount of neurons is to small to allow for any conclusions whether the change is more prominent in the right (lesioned) hemisphere than in the left (healthy). All percentages are as high as well above 60% for Dyskinesia Recording 4 except from that for the Fano factor (FF). The feature that best differentiate the baseline from post levodopa state is the entropy (H) for which 93% of all neurons exhibit a significant change in feature values.

Dyskinesia Recording 7, Table 5.2, has results based on 71 neurons in the left (healthy) hemisphere and 35 in the right (lesioned). Note that seven of the features exhibit a more significant change in the right hemisphere than in the left whereas 10 of them exhibit a more significant change in the left. Also note that, for four of the neurons, the percentages between left and right hemisphere differ only by three or less.

Feature	**Rec. 4 All** (15 neurons)	**Rec. 4 Left** (12 neurons)	**Rec. 4 Right** (3 neurons)
$<\mathbf{r}>$	80%	83%	67%
$\sigma^2_{\mathbf{r}}$	80%	75%	100%
$<\mathbf{n}>$	80%	83%	67%
$\sigma^2_{\mathbf{n}}$	80%	75%	100%
FF	47%	42%	67%
CV	73%	67%	100%
$<\mathbf{CV_2}>$	67%	75%	33%
$\sigma^2_{\mathbf{CV_2}}$	67%	67%	67%
$<\mathbf{LV}>$	80%	83%	67%
$\sigma^2_{\mathbf{LV}}$	73%	75%	67%
$<\mathbf{IR}>$	67%	75%	33%
$\sigma^2_{\mathbf{IR}}$	73%	75%	67%
$<\mathbf{SI}>$	80%	83%	67%
$\sigma^2_{\mathbf{SI}}$	73%	75%	67%
H	93%	92%	100%
TM	80%	83%	67%
IM	87%	83%	100%

Table 5.1: Table showing the percentage of neurons in Dyskinesia Recording 4 that exhibit a significant change in feature values after the injection of levodopa in comparison to before.

The percentages of all neurons that exhibit significant changes post levodopa are higher than, or equal to, 65% for all features. The feature that best differentiates the baseline from the post levodopa state are the rate average ($<r>$) and spike count average ($<n>$), with percentages of 90%, and the lowest performing feature is the local variation variance (σ^2_{LV}), with a percentage of 65%.

Feature	**Rec. 7 All** (106 neurons)	**Rec. 7 Left** (71 neurons)	**Rec. 7 Right** (35 neurons)
$<\mathbf{r}>$	90%	87%	94%
$\sigma^2_{\mathbf{r}}$	72%	79%	57%
$<\mathbf{n}>$	90%	87%	94%
$\sigma^2_{\mathbf{n}}$	72%	79%	57%
FF	76%	79%	71%
CV	82%	79%	89%
$<\mathbf{CV_2}>$	81%	82%	80%
$\sigma^2_{\mathbf{CV_2}}$	70%	70%	69%
$<\mathbf{LV}>$	75%	79%	69%
$\sigma^2_{\mathbf{LV}}$	65%	69%	57%
$<\mathbf{IR}>$	75%	76%	71%
$\sigma^2_{\mathbf{IR}}$	69%	72%	63%
$<\mathbf{SI}>$	76%	76%	77%
$\sigma^2_{\mathbf{SI}}$	71%	69%	74%
H	85%	86%	83%
TM	80%	77%	86%
IM	85%	83%	89%

Table 5.2: Table showing the percentage of neurons in Dyskinesia Recording 7 that exhibit a significant change in feature values after the injection of levodopa in comparison to before.

Remember that the highest and lowest performing features for Dyskinesia Recording 4 were the entropy (H) and the Fano factor (FF) respectively. For Dyskinesia Recording 7 there are three features that has higher, or equal, performance than the entropy and five features that has lower, or equal, performance than the Fano factor. However, note that the features performing well for Dyskinesia Recording 7 also have a better performance for Dyskinesia Recording 4, e.g. the rate average ($< r >$), spike count average ($< n >$), entropy (H) and local irregularity measure average ($< IM >$). The features with poor performance for Dyskinesia Recording 7 also have a worse performance for Dyskinesia Recording 4, e.g. local variation variance (σ^2_{LV}), local irregularity measure variance (σ^2_{IR}), local coefficient of variation variance ($\sigma^2_{CV_2}$) and local spiking irregularity measure variance (σ^2_{SI}).

5.2 Dimensionality Reduction

In Fig. 5.10, visualisations of the projection matrices $\boldsymbol{P}$ (see Sec. 4.4) used for PCA are presented for Dyskinesia Recording 4 and 7 (right). Red colours correspond to larger weights, whereas blue colours correspond to smaller. Note that all values are the absolute values of the weights, which means that the principal component space is largely based on the weights in a reddish colour. The figure also show the principal component variances (left).

The reduced feature spaces (see Sec. 4.4) were based on the results for the projection matrices and principal component variances. The amount of features used for the two reduced feature spaces were one and two, respectively. These number of features were purely based on the results for the principal component variances: Note that *one* principal component covers about 98% and 96% of the original feature space variance for Dyskinesia Recording 4 and 7, respectively, see Fig. 5.10 (left), i.e. *one* column of the projected feature space matrix ($\boldsymbol{F}_P$) were chosen to create the first reduced principal component space. Further, note that *two* principal components cover more than 99% of the original feature space variance for both recordings, i.e. the *two* first columns of the projected feature space matrix ($\boldsymbol{F}_P$) were chosen to create the second reduced principal component space.

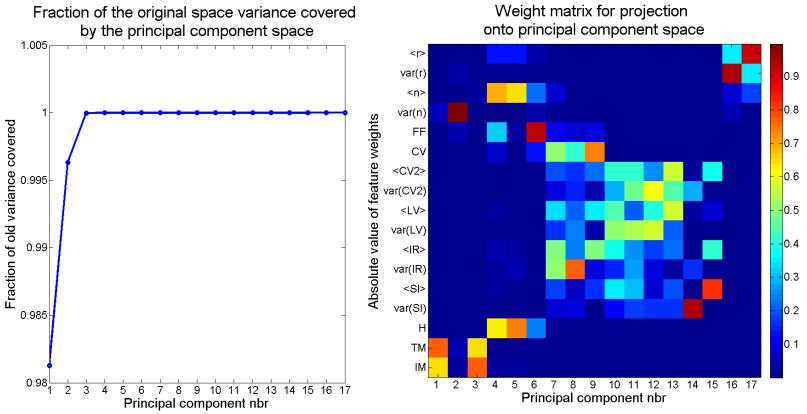

(a)

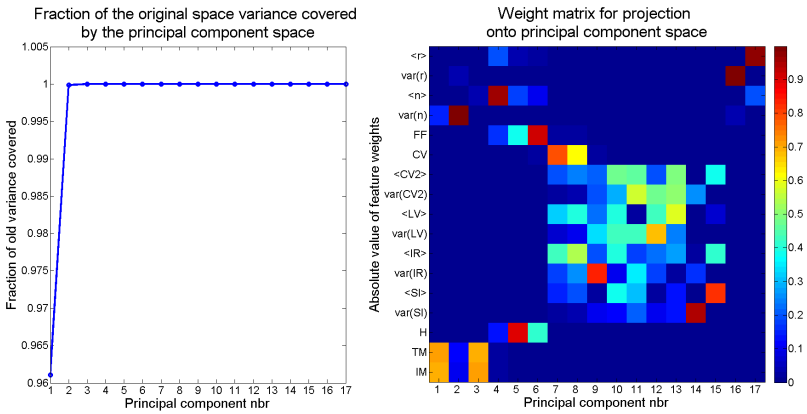

(b)

Figure 5.10: The cumulative fraction of the original feature space variance covered by the principal components (left) and the absolute value of the principal component coefficients, $|\boldsymbol{P}|$, (right) for Dyskinesia Recording 4 **(a)** and 7 **(b)**. $\boldsymbol{P}$ is the projection matrix used for the projection to the principal component space whose every column represent a principal component. The first column covers the largest amount of variance in the original data, the second the next largest and so on.

As for the reduced feature space (again, see Sec. 4.4), the number of features used were also decided from the results of the principal component variance, i.e. *one* for the first reduced feature space and *two* for

the second reduced feature space. The projection matrices show which of the features that were chosen for the two reduced feature spaces respectively: For the feature space reduced to *one* feature, the spike time metric (TM) has been used (largest weight in column one) and for the feature space reduced to *two* features the spike time metric, TM, (largest weight in column one) and the number of spikes variance, σ_n^2 or in the plot var(n), (largest weight in column two) has been used.

Another feature with a large weight in column one of the projection matrices is the spike interval metric (IM). Note that these three features (TM, σ_n^2 and IM) all have larger percentages for the right (lesioned) hemisphere than for the left (healthy) one, see Table 5.2. The same can not be said for Dyskinesia Recording 4, Table 5.1, but remember that it only contains recordings from 3 neurons in the right (lesioned) hemisphere. Also note that the matrix for Dyskinesia Recording 4, Fig. 5.10a (right), and that for Dyskinesia Recording 7, Fig. 5.10b (right), are alike: features with large weights for Rec. 4 has large weights for Rec 7. and vice versa. This, in extension, means that the data for Rec. 4 is alike that of Rec. 7.

5.3 Clustering

Analysis of the Number of Clusters

In Fig. 5.11 - 5.14, the within- and between-cluster scattering for Dyskinesia Recording 4 and 7 are presented for an increased number of clusters (1:15). For each of the plots, the cluster scattering as well as its derivative are included. Note, most clearly seen in the plots of the derivatives, that the cluster scattering change is largest when the number of clusters are increased from one to two and from two to three clusters (first to measure points of all derivative plots). This motivates the choice of the number of clusters as two and three.

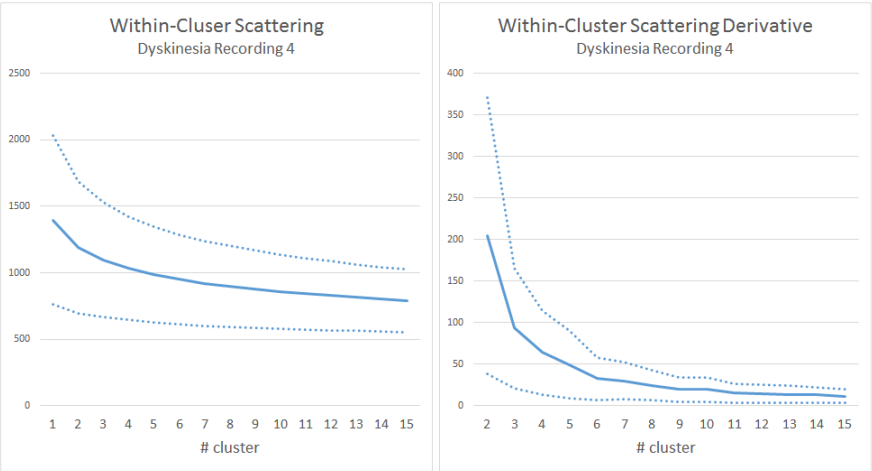

Figure 5.11: The within-cluster scattering (left) and its derivative (right) for an increased number of maximum clusters (1:15) of Dyskinesia Recording 4.

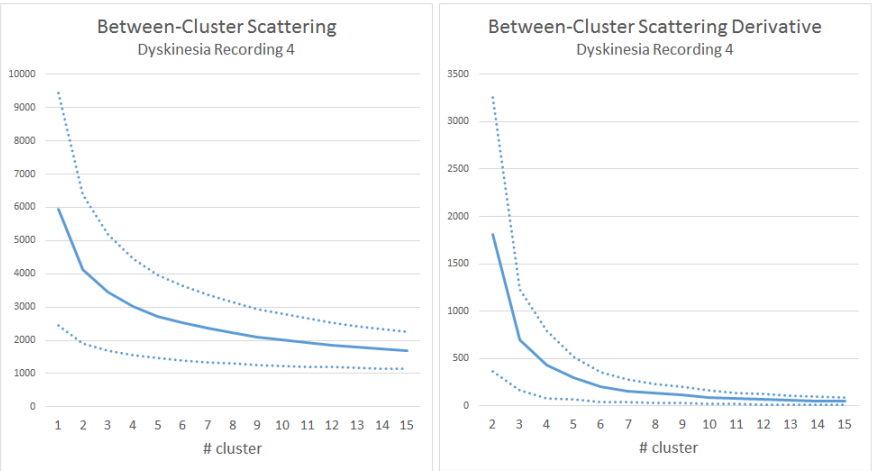

Figure 5.12: The between-cluster scattering (left) and its derivative (right) for an increased number of clusters (1:15) of Dyskinesia Recording 4.

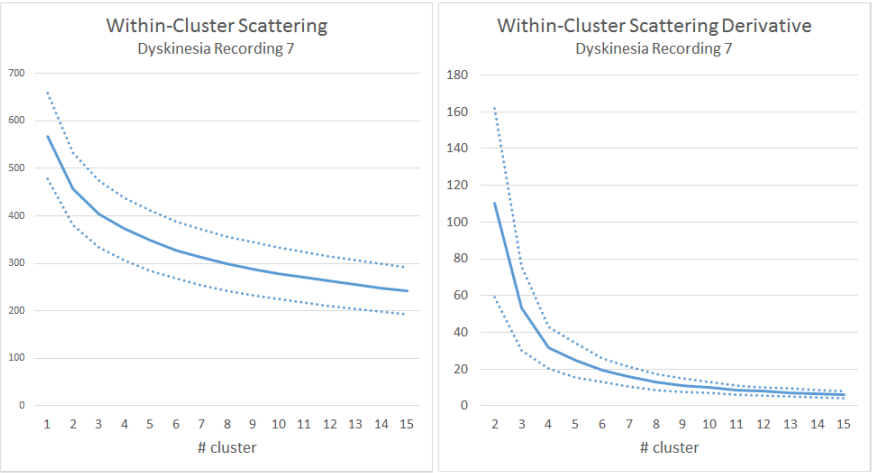

Figure 5.13: The within-cluster scattering (left) and its derivative (right) for an increased number of maximum clusters (1:15) of Dyskinesia Recording 7.

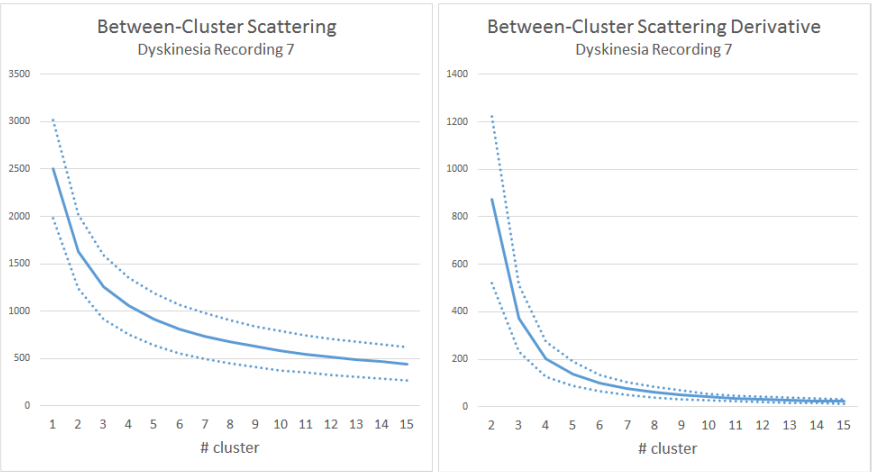

Figure 5.14: The between-cluster scattering (left) and its derivative (right) for an increased number of clusters (1:15) of Dyskinesia Recording 7.

Clustering to two states: (1) basline (2) post levodopa injection

In Figs. 5.15 and 5.16 a visualisation of the performance of the clustering for Dyskinesia Recording 4 is presented in the form of box plots. The boxes are separated by the median, the upper (yellow) part is the 25th percentile, the lower part (gray) is the 75th percentile and the error bars' upper and lower limits are the maximum and minimum values respectively.

The plots include cluster results for the recording with both 5 and 30 min of data post levodopa injection of levodopa removed and a comparison between the clustering in different feature spaces. Each box contains the fraction of correctly clustered segments for all neurons. Fig. 5.15 shows the clustering performance over the whole recording whereas Fig. 5.16 shows the clustering performance for the pre and post injection data separately.

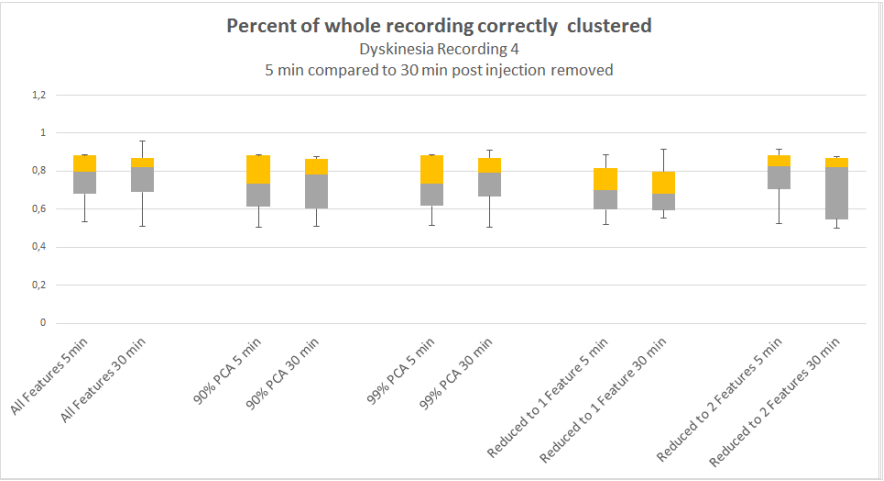

Figure 5.15: Clustering performance for two clusters over the whole recording Dyskinesia Recording 4 for different feature spaces. Every box contains the fraction of all neurons correctly clustered into the pre and post levodopa state and each pair of boxes is a comparison between 5 min and 30 min of data post levodopa removed.

Note that the performance measured over the whole recording, Fig. 5.15, generally high performance, with almost all boxes above 60%, which is also true for the post injection part of the data, Fig. 5.16b. The performance for the pre injection part of the data, Fig. 5.16a, exhibits a large variance (high boxes covering a large part of the fraction interval [0,1]). Note that the low performance in the clustering of the pre injection data in comparison to the post injection data is due to the fact that the dataset is unbalanced: The largest part of the recording duration is post levodopa injection. This means that the neurons clustered to one single cluster boost the performance for the post injection data, contributing with 100% correctly clustered segments, and worsens the results for the pre injection data, contributing with a 0% correctly clustered segments. To be clear, this difference in performance between the pre and post injection data does not mean that the post injection part of the data is easier clustered than the pre injection part.

Also note that the difference in performance between the clustering of the data with 5 and 30 min post levodopa injection removed is not large (compare first box of every pair to the second) and that the performance are not significantly worsened by reducing the feature space (compare first pair of boxes with the other pairs).

In Figs. 5.17 and 5.18 a visualisation of the performance of the clustering for Dyskinesia Recording 7 is presented. The plots include cluster results for the recording with both 5 and 30 min of data post levodopa injection removed and a comparison between the clustering in different feature spaces. In each box, the fraction of correctly clustered segments for all neurons are gathered.

Fig. 5.17a shows the clustering performance over the whole recording for all neurons and Fig. 5.17b the clustering performance over the whole recording for the 50 neurons that had the largest amount of time segments correctly clustered. Note that the performance of the clustering for the data with 30 min post levodopa injection removed are generally better than that of the data with 5 min removed (first box of each pair of boxes are lower than the second). Also note that the performance is worsened, although still good, when reducing the feature space for the data with 30 min post injection removed (com-

pare the second box of the first pair with all second boxes in Fig. 5.17a and 5.17b). Note that the worsening of the performance is even more prominent for the 50 top performing neurons in Fig. 5.17b when reducing the feature space.

Fig. 5.18 shows the clustering performance for the pre and post injection data separately. Note that the values are generally high for the post injection data, Fig. 5.18b whereas they are around 40% to 80% for the pre injection data, Fig. 5.18a. This difference is, as for Dyskinesia Recording 4, due to the fact that the largest part of the recording duration is post levodopa injection, i.e. the difference in performance should not be interpreted as the post injection part of the data being easier to cluster than the pre injection part.

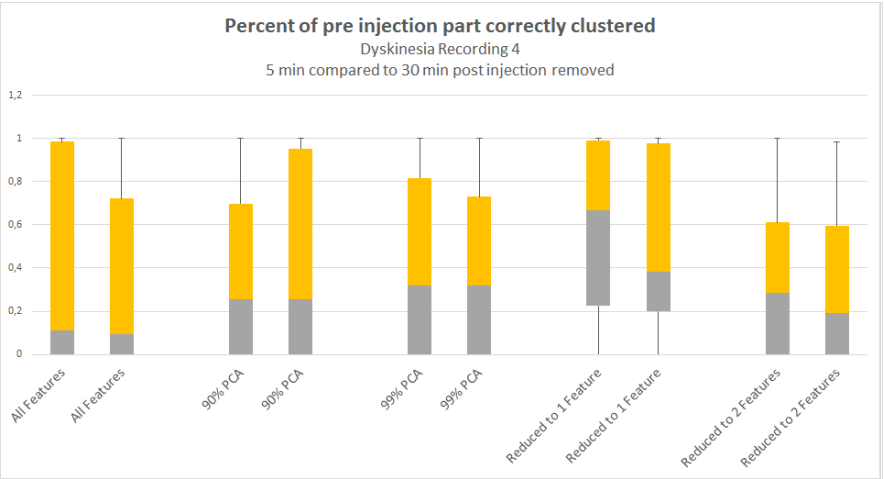

(a)

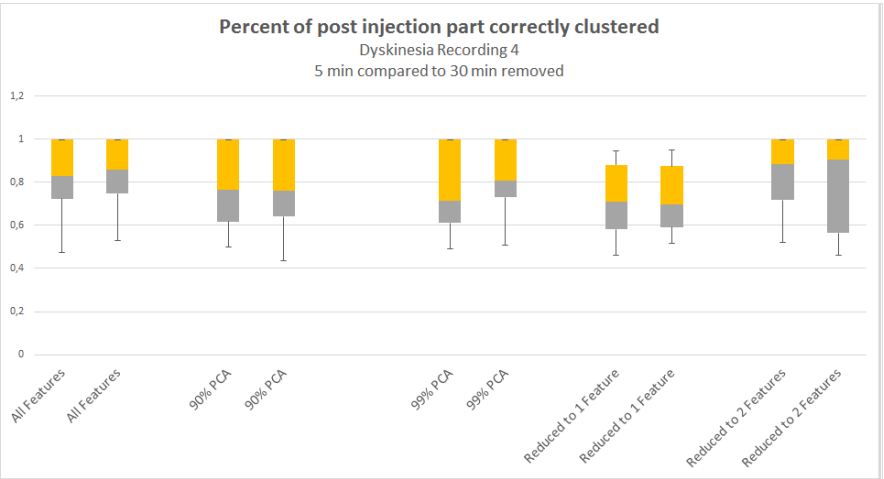

(b)

Figure 5.16: Clustering performance for two clusters on pre **(a)** and post **(b)** injection data from Dyskinesia Recording 4 for different feature spaces. Every box contains the fraction of all neurons correctly clustered into the pre or post levodopa state and each pair of boxes is a comparison between 5 min and 30 min of data post levodopa removed.

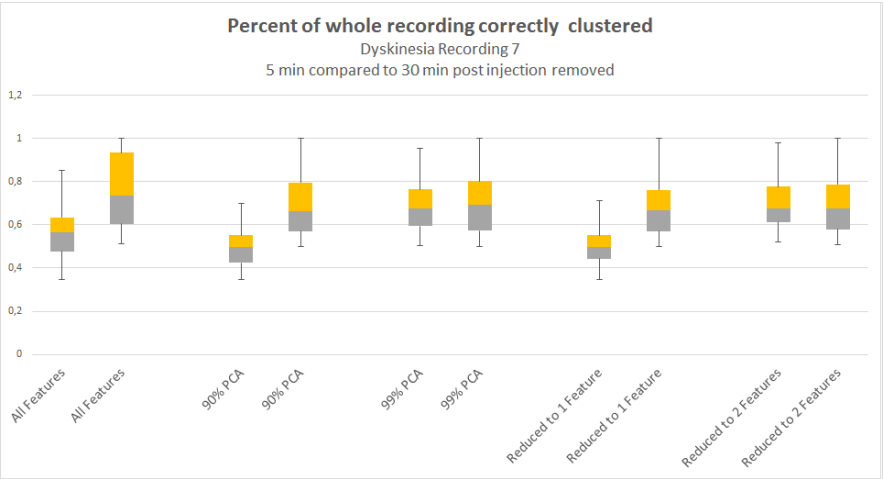

(a)

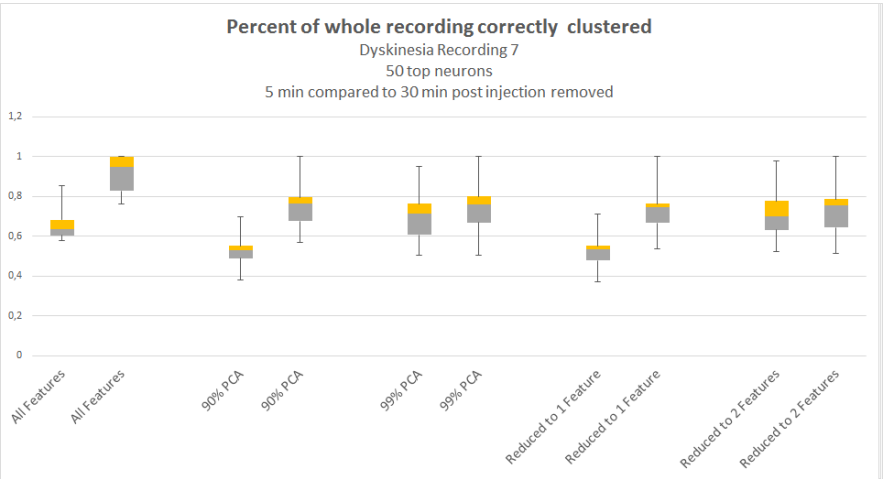

(b)

Figure 5.17: Clustering performance for two clusters, on the whole recording for all neurons **(a)** and the 50 neurons that that had the largest amount of time segments correctly clustered **(b)**, of Dyskinesia Recording 7 for different feature spaces. Every box contains the fraction of all neurons correctly clustered into the pre or post levodopa state and each pair of boxes is a comparison between 5 min and 30 min of data post levodopa removed.

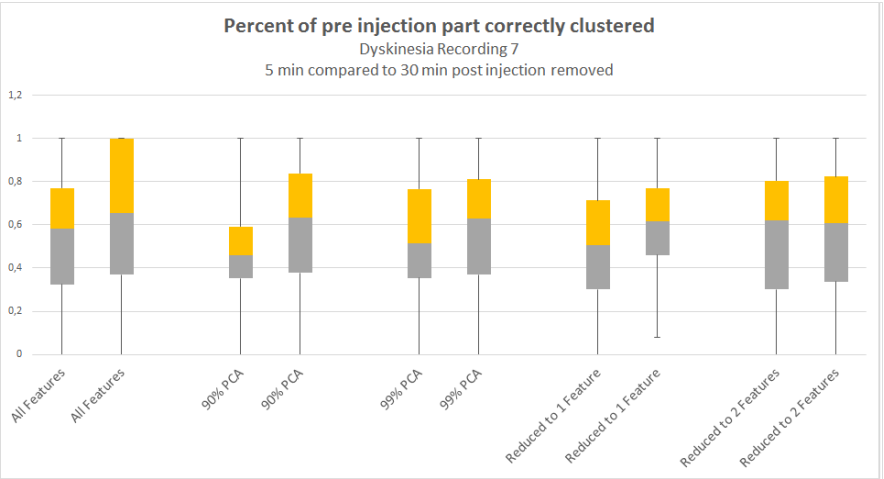

(a)

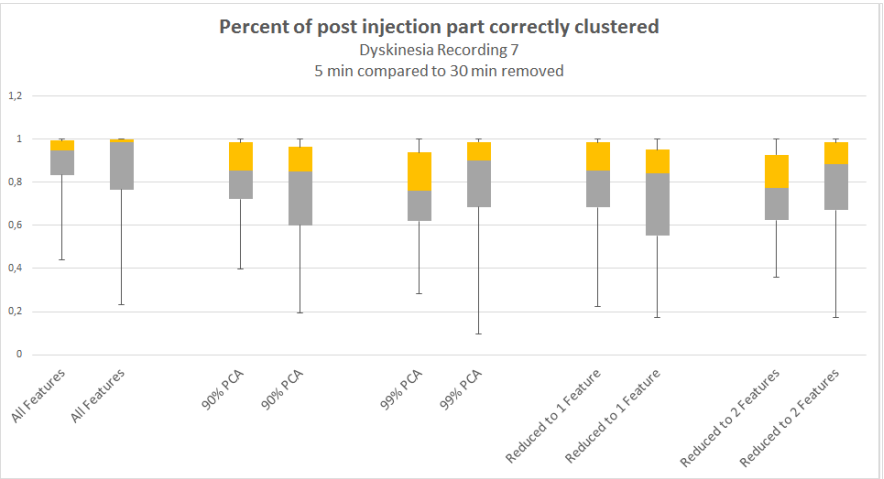

(b)

Figure 5.18: Clustering performance for two clusters on pre **(a)** and post **(b)** injection data from Dyskinesia Recording 7 for different feature spaces. Every box contains the fraction of all neurons correctly clustered into the pre or post levodopa state and each pair of boxes is a comparison between 5 min and 30 min of data post levodopa removed.

Clustering to three states: (1) basline, (2) transistion state and (3) post levodopa injection

The clustering to three states chosen as pre injection state, transition state and post injection state were also measured in the fraction of the states that were correctly clustered. When dividing the states into these three groups the mean fraction over all neurons that were correctly clustered for Dyskinesia Recording 4 were 64,7%. For each state the correctly clustered mean fraction of segments for were: (1) 28,3%, (2) 76,9% and (3) 24,8%. For Dyskinesia Recording 7 the mean fraction over all neurons that were correctly clustered were 55,8%. For each state the correctly clustered mean fraction of segments were: (1) 55,4%, (2) 71,0% and (3) 39,4%. Note that the transistion state (2) has the highest percentage of correctly clustered segments, although not very high and that the performance of clustering to the pre injection (1) and post injection state (3) are low.

When dividing the states into two groups instead: (1) pre injection state and (2) transistion state plus post injection state, the mean percentage over all neurons that were correctly clustered for Dyskinesia Recording 4 were 82,9%. For each group the correctly clustered mean percentage of segments for were: (1) 28,3% and (2) 89,9%. For Dyskinesia Recording 7 the mean percentage over all neurons that were correctly clustered were 76,5%. For each group the correctly clustered mean fraction of segments were: (1) 55,4% and (2) 89,9%. Note that the percentage for the pre injection state (1) are low whereas the percentage for the combined post injection state is high, indicating that the problem was not simply to distinguish between the transition state and post injection state.

5.4 Classification

Classification of two states: (1) baseline and (2) post levodopa injection

In Fig. 5.19, the classification performance measured in fraction of time segments correctly classified are presented. Each box holds the gathered performance for all neurons for both Dyskinesia Recording 4, Fig. 5.19a and 7, Fig. 5.19b, and results from all neurons (first pair of

boxes), nerouns in the left (healthy) hemisphere (second pair of boxes) and neurons in the right (lesioned) hemisphere (third pair of boxes). Note that the results for the right hemisphere of Rec. 4 are based on three neurons alone, hence the small or non existing error bars and large variance.

Note that the performance is generally higher (small and highly placed boxes) for the post injection part of the data for Rec. 4, Fig. 5.19a, whereas there is no significant difference in performance between the pre injection and post injection part of the data for Rec. 7, Fig. 5.19b. Also note that the performance of the classification are generally higher for Rec. 7 (all boxes well above 0,8) than for Rec. 4 and that the classification performance does not significantly differ between the left (healthy) and right (lesioned) hemisphere for Rec. 7.

Classification of three states: (1) baseline, (2) transistion state and (3) post levodopa injection

In Fig. 5.20, the classification performance measured in fraction of time segments correctly classified are presented. Note, again, that the results for the right (lesioned) hemisphere of Dyskinesia Recording 4 are based on three neurons alone.

The classification performance is generally higher for the pre and post-end injection part of the data (first and third box of each triplet) from Rec. 4, Fig. 5.20a, than for the transition state (second box of each triplet). However, the performance for the post-end injection data is still low, indicating that the problem in the post injection part (combined transition and post injection state) is not to distinguish between the the transition state and post-end injection state.

The low performance of the classification of the two post injection states is even more evident in the results for Dyskinesia Recording 7, Fig. 5.20b (second and third box of each triplet low). Note that there is no significant difference in performance of classification between the left (healthy) and the right (lesioned) hemisphere.

(a)

(b)

Figure 5.19: Classification performance for Dyskinesia Recording 4 **(a)** and 7 **(b)** using two states for classification. Every box contains the fraction of all neurons correctly classified into the pre and post levodopa state. Each pair shows the pre and post injection classification performance for all neurons, neurons from the left hemisphere and neurons from the right hemisphere respectively.

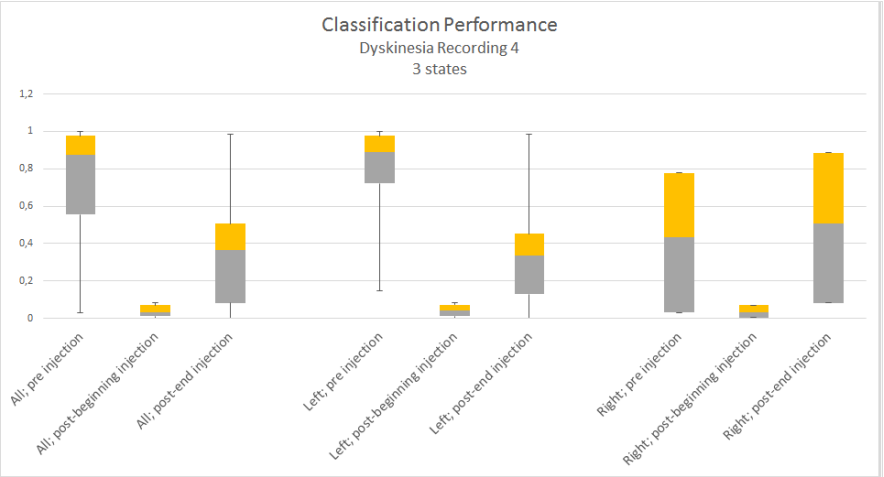

(a)

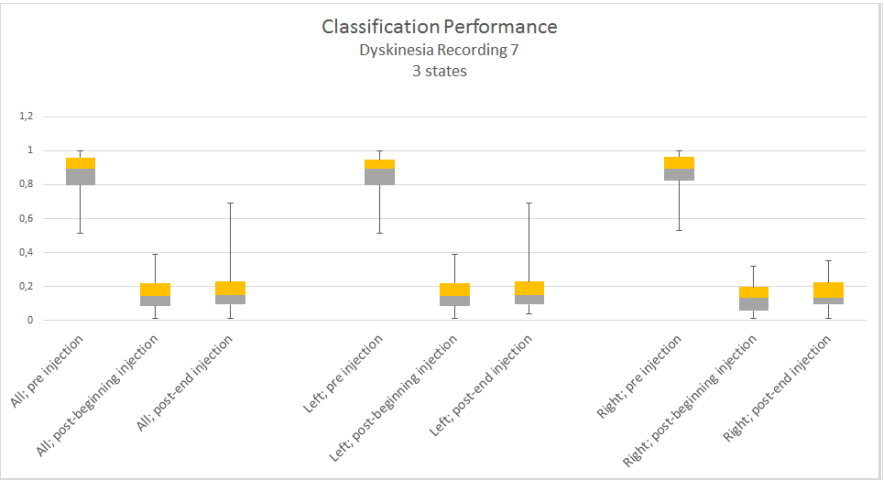

(b)

Figure 5.20: Classification performance for Dyskinesia Recording 4 **(a)** and 7 **(b)** using 3 states for classification. Every box contains the fraction of all neurons correctly classified into the baseline, transition state and post levodopa state. Each pair shows the pre, middle and post injection classification performance for all neurons, neurons from the left hemisphere and neurons from the right hemisphere respectively.

6

Discussion

In this thesis work, a large number of features has been extracted from the data recorded with novel electrodes at NRC. The assumption that a dynamic change in the neural activity can be related to changes between the pre and post levodopa state has been further strengthened. As was expected, the feature extraction showed that it is not sufficient to study a single neuron, as different neurons behave differently. This can be seen in Figs. 5.1-5.9 where some neurons exhibit significant changes in feature values post levodopa (both increased and decreased), whereas others do not exhibit a significant change.

The summary of the feature extraction results (see e.g. Table 5.2) however, show that a population of neurons can clearly prove a mathematical difference between the pre and post levodopa state. What can be considered as somewhat surprising is that there were no general differences between the left (healthy) and right (lesioned) hemisphere in terms of the fraction of neurons exhibiting a significant feature value change post levodopa. This can be seen in Table 5.2 where some percentages are higher for the left (helthy) hemisphere, whereas others are higher for the right (lesioned) hemisphere. The one result showing a noticable difference for the three large weight features of PCA (TM, σ_n^2 and IM), which all had higher percentages for the right (lesioned) hemisphere than the left (healthy) one, see Table 5.2. This *could* indicate that the difference between pre and post levodopa state is easier to detect in the lesioned hemisphere.

Adding to the variation of behaviour within the right and left hemisphere, there also seem to be a variation in neurons within the same

site, see e.g. Fig. 5.1 *RFA; Left*. The variation within the right and left hemisphere as well as within the same site is found in all feature extraction results, Fig. 5.1-5.9, except for the entropy results found in Fig. 5.9, for which all neurons exhibit an increase of feature values post levodopa. Unfortunately, because the variations mentioned exist for all features except one (for which this seem to be a coincidence since the same result was not found for Dyskinesia Recording 7) it is difficult to, mathematically, draw a general conclusion of how the brain behave during the post levodopa state as compared to the baseline. What one *can* say, based on the results, is that there is a significant difference in behaviour of the neurons between the baseline and post levodopa state, and that this difference can be mathematically quantified.

To handle the large amount of data has been a challenge through the whole work process: From how to perform the segmentation to extracting features and their subsequent clustering and classification, and finally to interpret and present the results. The fact that different neurons behave differently, in terms of the features applied here, may motivate one to study the results on a neuron to neuron basis. However, because of the large amount of neurons, the extended recording duration and the fact that for every neuron, 17 features were extracted, it was rather difficult to study and present on that level of detail. But, in spite of the difficulties faced with the amount of data, the results for the feature extraction based on Dyskinesia Recording 4 and 7 can be considered satisfactory: All features for Dyskinesia Recording 7 exhibited a significant change in feature values after the injection of levodopa for a clear majority of the neruons, see Table 5.2.

The difference in behaviour between neurons did not only complicate the presentation and interpretation of the results: The nature of some neurons, specifically the fact that there were particularly silent neurons, made the differentiation between different states difficult. The reasons for the silence may be that either the signals were not properly picked up by the recording, or that these neurons simply does not fire a lot of action potentials: In the striatum, e.g., there are neurons that are mostly silent. The reason why, e.g., the silent neurons posed a problem in terms of the feature extraction was that many of the features were formulated so that they required a certain amount

of activity, i.e. a sufficient amount of action potentials fired, to be reliably calculated: For example, if there is not enough activity, the average or variance values run the risk of becoming biased. To regulate the amount of data that the feature value for each segment was based on the length of the time window was changed. This, however, proved to introduce yet another difficulty: How to choose this time window?

Some of the features, specifically those which were based on the average and variance, were sensitive to the length of the time window used for segmentation. The use of an overlap offered a larger amount of segments to use for analysis with the drawback that multiple of segments contained more or less the same data. A short time window rules out a lot of the features because it results in an insufficient amount of activity to calculate the feature values. A longer time window results in there not being enough segments to differ states from each other and that more transient states cannot be differentiated: If the time window is too long, it results in segments containing states that one wishes to distinguish from each other. This, of course, makes it difficult to assign a single state to that segment of time and the states are "drowned" within the segments.

The choice of time window length were purely based on the timescale of the state that were investigated. To find subclusters within the baseline and post levodopa state that could be connected to events such as start or stop of locomotion was not possible for Dyskinesia Recordin 4 and 7 because the time window to differentiate the baseline from the post levodopa state were too long. However, this was not the main goal with the analysis of these recordings and if the time window had been shortened there may not have been a sufficient number of features left to perform a successful clustering or classification.

The decrease of the dimensionality of the feature space showed that the performance of the clustering did worsen, even if this was not very significant (see, e.g., Fig. 5.17a). This suggests that some of the features are redundant, which is probably due to the large correlation between some of them: For example, the rate and number of spikes differ only by a constant. The same conclusions could, i.e., be drawn using a significantly reduced number of features, as the reduction to as

few as two features still delivered a satisfactory result. Another way to reduce the feature space could have been to group the features according to the correlation between them and choose one of the features in each group for the new reduced feature space. This would, however, have called for an additional analysis of which of these features were the most suitable one to use in each group.

The results for the clustering to three states (see Sec. 5.3) showed that it is difficult to find a transition state directly after injection when the dyskinesia is gradually developing. This is even more apparent when performing classification: Even when *a priori* stating that this state exists it could not be easily found. This is, however, not very surprising: Because the dyskinesia is gradually developing during the transition state there is no reason to believe that the neural activity is stationary enough for a separate state to be distinguished.

The work to differentiate the smaller time scale states, such as start and stop of locomotion, for Open Field Recording 8 and 36 were begun but unfortunately, the problems stated above proved even more challenging for this application: The smaller timescale forces one to study the data in smaller time windows, which naturally presents one with less data to analyse within each window. This eliminates a lot of the features because of the lacking amount of data to calculate, e.g., unbiased mean and variance.

One question is if there is a transient change of neural activity prior to the start or stop of locomotion, or if locomotion as opposed to no movement could be differentiated from each other. The supposed transient change is believed to occur on a subsecond scale. This calls for a subsecond length of the time window for segmentation which for some events left one with no spikes at all within some segments. One advantage of the Open Field Recordings, however, is that the amount of events noted enables the use of repeated trials by cutting out and timing windows around each event. This should be done with caution of how precise the annotation of the start and stop of locomotion in comparison to the assumed timescale of the state one wishes to detect.

One way to increase the time resolution, i.e., shorten the time window

for segmentation could be to not use the average or variance for the rate (r), spike count (n) and local measures of variability (CV_2, LV, IR and SI). While decreasing the length of the time window for these features the others (FF, CV, H, TM and IM) can still be calculated on a larger time window: If one wishes to use all features together at a higher time resolution, one can simply let these features' values remain constant in the duration corresponding to several shorter time windows. What is important to remember, however, is that decreasing the time window for segmentation *too* much can still affect the rate, spike count and local measures of variation, even if their average or variance is not used. For example a very small time window would, for the rate, result in a lot of segments not containing any spikes at all whereas some contain a single one. The segments containing one single spike would have very large rate denoted: Imagine, e.g., that the time window is 10^{-3} s and that one single spike was recorded in the duration of 1 second. This would result in 999 segments within the 1 second denoting the rate 0 spikes/s, whereas one would denote $1/10^{-3} = 1000$ spikes/s. As the Fano factor (FF) and coefficient of variation (CV) are based on the rate they will consequently be affected by a too small time window as well. However, there are methods to make these measures less dependent of the firing rate that can be investigated, see e.g. [29] for more information.

7

Conclusions

The analysis of the features show that there is a significant difference between the baseline and post levodopa state. This can be considered an interesting result for the overall goal to explore methods for feature extraction. It is obvious that different neurons react in different ways: Some of the neurons, e.g., become significantly more active whereas others are more silent after the injection than before, and some neurons do not seem to either increase or decrease their activity. This confirms the need for studying a population of neurons as opposed to single neurons separately. In this case, studying a single neuron could very well have been misleading in the search for the underlying biological mechanism.

Bibliography

[1] J. P. Cunningham and B. M. Yu, *Dimensionality reduction for large scale neural recordings*. Nature America, 2014.

[2] *What is Data Mining (Predictive Analytics, Big Data)*. `http://www.statsoft.com/Textbook/...` `...Data-Mining-Techniques#mining` (Fetched September 2014)

[3] O. Shmiel *et. al*, *Processing of Multichannel Recordings for Data-Mining Algorithms*. IEEE Transactions on Biomedical Engineering, Vol. 54, No. 3, March 2007.

[4] E. O. Widmaier, H. Raff and K. T. Strang, *Vander's Human Physiology: The Mechanisms of Body Function, Twelfth Edition*. McGraw-Hill Companies, Inc., 2011.

[5] P. Halje, M. Tamtè *et. al.*, *Levodopa-Induced Dyskinesia Is Strongly Associated with Resonant Cortical Oscillations*. The Journal of Neuroscience, 32(47) pp. 16541-16551, September 2012.

[6] L. Sörnmo and P. Laguna, *Bioelectrical Signal Processing in Cardiac and Neurological Applications*. Elsevier Inc., 2005.

[7] *Chemical synapse schema cropped*, `http://en.wikipedia.org/wiki/Neuron` (Fetched October 2014)

[8] P. Dayan and L.F. Abbott, *Theoretical Neuroscience: Computational and Mathematical Modeling of Neural Systems*. Massachusettes Institute of Technology, 2001.

[9] D. Purves *et al.*, *Neuroscience, Third Edition* Sinauer Associates Inc., 2004.

[10] *Action Potential*, `http://en.wikipedia.org/wiki/Action_potential` (Fetched October 2014)

[11] *Basal-ganglia-coronal-sections-large* `http://en.wikipedia.org/wiki/Basal_ganglia` (Fetched October 2014)

[12] Web MD, Brain & Nervous System Health Center: Parkinson's Disease Health Center *Glossary of Parkinson's Disease Terms* `http://www.webmd.com/parkinsons-disease/...` `...parkinsons-glossary?page=2` (Fetched September 2014)

[13] *Hyperkinetic*, `http://www.merriam-webster.com/...` `...dictionary/hyperkinetic` (Fetched October 2014)

[14] *Dystonic*, `http://www.merriam-webster.com/...` `dictionary/dystonic` (Fetched October 2014)

[15] T. Rydèn and G. Lindgren, *Markovprocesser*. Lund University, 2000.

[16] M. Nawrot, A. Aertsen and S. Rotter, *Single-trial estimation of neuronal firing rates: From single-neuron spike trains to population activity*. Journal of Neuroscience Mothods 94, pp. 81-92, 1999.

[17] N. Ivica and M. Tamtè M. Ahmed, U. Richter, and P. Petersson, *Design of a high-density multi-channel electrode for multi-structure parallel recordings in rodents*. 36th Annual International Conference of the IEEE Engineering in Medicine and Biology Society, Chicago, USA, 2014.

[18] *Anterolateral*, `http://www.merriam-webster.com/...` `...medical/anterolateral` (Fetched December 2014)

[19] M.S. Fee, P.P. Mitra, D. and Kleinfeld *Automatic sorting of multiple unit neuronal signals in the presence of anisotropic and non-Gaussian variability*. J. Neurosci. Methods 69, 175-188, 1996

[20] K. Rajdl and P. Lansky, *Fano Factor Estimation.* Mathematical Biosciences and Engineering, Vol. 11, Nbr. 1, pp. 105-123, February 2014.

[21] A. Ponce-Alvarrez, B. E. Kilavik and A. Riehle, *Comparison of local measures of spike time irregularity and relating variability to firing rate in motor cortical neurons.* J Comput Neurosci (2010) 29:351-365, 2009.

[22] S. Grün and S. Rotter, *Springer Series in Computational Neuroscience 7*, DOI `10.1007/978-1-4419-5675-0_13`, 2010.

[23] J. D. Victor, *Approaches to Information-Theoretic Analysis of Neural Activity.* Biol Theory 2006 ; 1(3):302-316, 2006.

[24] M. Abeles *et al.*, *Cortical activity flips among quasi-stationary states.* Proc. Natl. Acad. Sci. USA, Vol. 92, pp. 8616-8620, September 1995.

[25] J. D. Victor, *Spike train metrics.* Current Opinion in Neurobiology 2005, 15:585-592, 2005.

[26] R. O. Duda, P. E. Hart and D. G. Stork, *Pattern Classification, Second Edition.* John Wiley & Sons, Inc., 2001

[27] *Clusters*, `http://en.wikipedia.org/wiki/File:Clusters.svg` (Fetched December 2014)

[28] *Hierarchical clustering simple diagram*, `http://en.wikipedia.org/wiki/File:Hierarchical_...` `...clustering_simple_diagram.svg` (Fetched December 2014)

[29] M.P. Nawrot. Analysis and Interpretation of Interval and Count Variability in Neural Spike Trains. In S. Grün and S. Rotter (eds.), *Analysis of Parallel Spike Trains*, Springer Series in Computational Neuroscience 7, 2010.